



# Geochemistry, Geophysics, Geosystems



#### RESEARCH ARTICLE

10.1029/2024GC011839

#### **Key Points:**

- Fiordland-derived crystalline basement units have been dissected and dextrally displaced ~70–90 km by the Alpine Fault since the late Pliocene
- The southern Alpine Fault has evolved within a distributed fault network and may be less mature than the more northern parts of the fault
- Structural complexity where many Holocene earthquakes have terminated appears consistent with structural segmentation of the fault

#### **Supporting Information:**

Supporting Information may be found in the online version of this article.

#### Correspondence to:

A. M. Mere, andre.mere@email.ucr.edu

#### Citation:

Mere, A. M., Barth, N. C., Schwartz, J. J., & Kylander-Clark, A. (2024). Slip history, tectonic evolution, and fault zone structure along the southern Alpine Fault, New Zealand. *Geochemistry, Geophysics, Geosystems*, 25, e2024GC011839. https://doi.org/10.1029/2024GC011839

Received 26 AUG 2024 Accepted 27 OCT 2024

#### **Author Contributions:**

Conceptualization: A. M. Mere, N. C. Barth Formal analysis: A. M. Mere, A. Kylander-Clark Investigation: A. M. Mere, N. C. Barth Supervision: N. C. Barth Visualization: A. M. Mere Writing – original draft: A. M. Mere Writing – review & editing: N. C. Barth, J. J. Schwartz

© 2024 The Author(s). Geochemistry, Geophysics, Geosystems published by Wiley Periodicals LLC on behalf of American Geophysical Union. This is an open access article under the terms of the Creative Commons Attribution License, which permits use, distribution and reproduction in any medium, provided the original work is properly cited.

# Slip History, Tectonic Evolution, and Fault Zone Structure Along the Southern Alpine Fault, New Zealand

A. M. Mere<sup>1</sup>, N. C. Barth<sup>1</sup>, J. J. Schwartz<sup>2</sup>, and A. Kylander-Clark<sup>3</sup>

<sup>1</sup>Department of Earth and Planetary Sciences, University of California Riverside, Riverside, CA, USA, <sup>2</sup>Department of Geological Sciences, California State University Northridge, Northridge, CA, USA, <sup>3</sup>Department of Earth Science, University of California Santa Barbara, Santa Barbara, CA, USA

**Abstract** The study of active fault zones is fundamental to understanding both long-term tectonics and short-term earthquake behavior. Here, we integrate lidar-enabled geomorphic-geologic mapping and petrochronological analysis to reveal the slip-history, tectonic evolution, and structure of the southern Alpine Fault in New Zealand. New petrographic, zircon U-Pb and zircon trace-element data from fault-displaced basement units provides constraint on ~70–90 km of right-lateral displacement on the presently active strand of the southern Alpine Fault, which we infer is of Plio-Quaternary age. This incremental displacement has accumulated while the offshore part of the fault has evolved within a distributed zone of plate boundary deformation. We hypothesize that pre-existing faults in the continental crust of the Pacific Plate have been exploited as components of this distributed plate boundary system. Along the onshore southern Alpine Fault, detailed mapping of active fault traces reveals complexity in geomorphic fault expression. Our analysis suggests that the major geomorphic features of the southern Alpine Fault correspond to penetrative fault zone structures. We emphasize the region immediately south of the central-southern section boundary, where a major extensional stepover and restraining bend are located along-strike of each other. We infer that this geometry may reflect segmentation of the Alpine Fault between two distinct fault segments. The ends of these proposed segments meet near where several Holocene earthquake ruptures have terminated. Our new constraints on the evolution and structure of the southern Alpine Fault help contribute to improved characterization of the greatest onshore source of earthquake hazard in New Zealand.

#### 1. Introduction

The characterization and understanding of active fault zones are fundamental parts of both tectonics and earth-quake hazards. In these applications, similar parameters may be investigated, such as the rates and styles of fault-accommodated deformation (e.g., Atwater, 1970; Dawson et al., 2013; Graham et al., 1989; Hatem et al., 2022; Hunt, 1978; Lamb, 2011; Litchfield et al., 2014; Little & Jones, 1998; Matti & Morton, 1993; Mere & McPhillips, 2024), the geometry of the fault network (e.g., Davey et al., 2007; Herman et al., 2009; P. R. King, 2000; Litchfield et al., 2018; Shuck et al., 2021; Stern et al., 2007; Stirling et al., 2017), and the degree of structural connectivity therein (e.g., Marshall et al., 2023; Seebeck et al., 2024). On the other hand, timescales of interest may vary markedly, with tectonic studies commonly focusing on long-term patterns and characteristics (Myr-scale) and those of earthquake hazards vice versa (kyr to yr-scale).

Despite these large differences in temporal scale, many fault properties are linked through time by the process of structural evolution, which is attendant to the accumulation of displacement. Specific evolutionary processes include fault tip propagation and segment linkage (Cowie & Scholz, 1992; Davis et al., 2005; Dawers et al., 1993; Naylor et al., 1986; Peacock & Sanderson, 1991), off-fault damage localization (Ben-Zion & Sammis, 2003; Manighetti et al., 2004), and geometric simplification (Childs et al., 2009; Stirling et al., 1996), amongst others. Because of these processes, faults are dynamic features with temporally and spatially variable properties. Fault structural maturity encompasses this relationship (Manighetti et al., 2007; Wesnousky, 1988) by linking long-term tectonic deformation and fault evolution to many fault properties that influence contemporary seismogenic behavior (Dolan & Haravitch, 2014; Faulkner et al., 2010; Perrin et al., 2016). For example, fault zone geometry is modified through time, dependent on the style of tectonic evolution, and serets a first-order control on earthquake hazard parameters such as the magnitudes, spatial distributions, and senses of coseismic displacements (Ando et al., 2017; Antoine et al., 2022; Elliott et al., 2015; Nevitt et al., 2023; Wan et al., 2016). Because

MERE ET AL. 1 of 34

15252027, 2024, 11, Downloaded from https://agupubs.onlinelibrary.viley.com/doi/10.1029/2024GC011839, Wiley Online Library on [12/03/2025]. See the Terms and Conditions (https://onlinelibrary.viley.com/terms-and-conditions) on Wiley Online Library for rules of use; OA

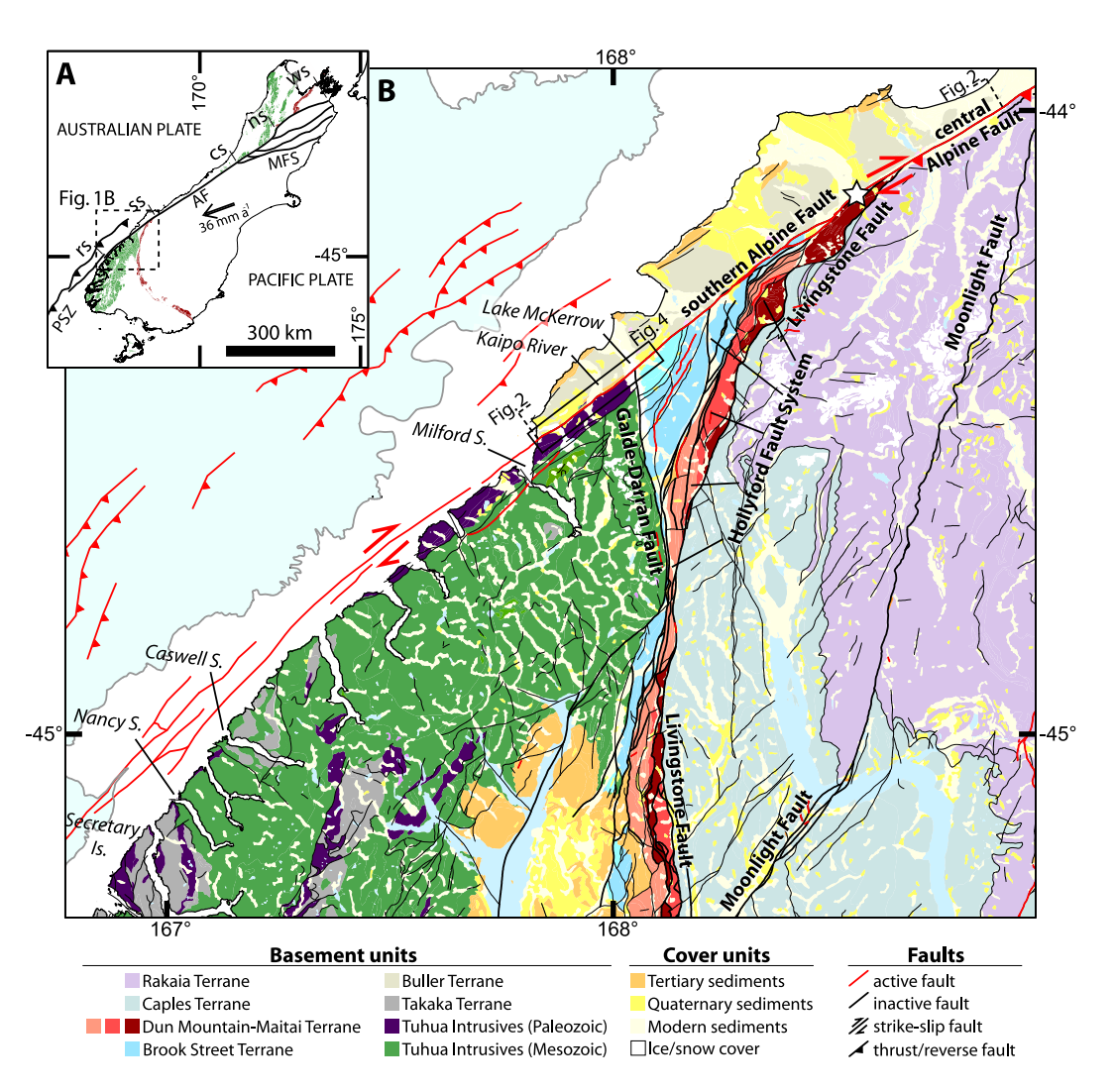


**Figure 1.** Tectonics and geological setting of the South Island of New Zealand. (a) Present-day tectonic setting of the South Island of New Zealand. Red and green shaded areas delimit the extent of the Dun-Mountain Maitai Terrane and Tuhua Intrusives, respectively, which have been dextrally offset by Cenozoic plate motion accommodated by the Alpine Fault. Thin lines perpendicular to the Alpine Fault delimit the northern boundaries of each Alpine Fault section: the Wairau section (ws), northern section (ns), central section (cs), southern section (ss), and Resolution section (rs). Arrow denotes the azimuth and velocity of geologically recent Australian-relative Pacific Plate motion calculated from DeMets et al. (1994) and DeMets and Dixon (1999). AF-Alpine Fault, MFS-Marlborough Fault System, PSZ-Puysegur Subduction Zone. (b) Geological setting of the study area and surrounding regions. Fault traces are shown as thick lines for major faults and thin lines for minor faults. Offshore gray line depicts the 2,000 m water depth isobath, which is the approximate location of the continental shelf. Onshore active faults are from Litchfield et al. (2014) and offshore from Barnes et al. (2002, 2005). Basement geology is simplified from Turnbull (2000), Cox and Barrell (2007), and Rattenbury et al. (2010). Is., Island; S., Sound.

long- and short-term tectonic processes may be related, there is value in characterizing the properties and evolutionary history of active faults across a variety of timescales.

In this contribution, we focus on the Alpine Fault, which is the active Pacific-Australian Plate boundary structure and likely the single greatest onshore source of earthquake hazard in the South Island of New Zealand (Howarth et al., 2021; Stirling et al., 2012). The Alpine Fault is frequently conceptualized as a highly mature intercontinental transform fault, meaning that its large magnitude of cumulative displacement has resulted in a high degree of damage localization, geometric simplification, and structural connectivity within the principal zone of displacement. This interpretation is based on research that has predominantly focused on the central part of the fault (e.g., Norris & Toy, 2014, references therein). However, a growing body of work shows that more southern parts of the fault have different properties (southern and Resolution sections, Figure 1). For instance, toward the

MERE ET AL. 2 of 34

15252027, 2024, 11, Downloaded from https

south, the kinematics and near-surface geometry of the fault changes markedly (Berryman et al., 1992; Norris & Cooper, 2001), the fault core widens, and shear fabrics within are less developed (Barth et al., 2013). In the same region, the deeper crustal geometry of the fault is much less constrained than farther to the north and is presently debated (cf., Howarth et al., 2021; Lamb et al., 2015; Warren-Smith et al., 2016, 2022), and little is known about its Cenozoic evolution. Offshore, seismic reflection data and tectonic reconstructions suggest that the presently active strand is much younger than its central counterpart (Barnes et al., 2005; Lamarche & Lebrun, 2000; Lebrun et al., 2000). Recent work on other major faults shows that structural maturity tends to decrease toward fault tips (Perrin et al., 2016), where cumulative displacement and fault age necessarily decrease toward zero (Scholz & Lawler, 2004). To date, the possibility that lateral variations in the properties of the Alpine Fault reflect a difference in how the southern parts of the fault have evolved, reflect different degrees of structural maturity, reflect differences in crustal geometry, or each of these, has received little attention.

Here we improve knowledge and understanding of the southern Alpine Fault by integrating lidar-enabled mapping of geomorphic fault expression, geologic field mapping of basement units and structures, and petrochronology of several distinctive crystalline basement units that are present within the southernmost part of the fault zone. This yields a diverse data set that we interpret together with many previous studies in and southwest of New Zealand; this allows for new constraint on the slip history, tectonic evolution, and structure of the southern Alpine Fault. For the first time, we present an estimate of dextral displacement on the presently active strand of the southern Alpine Fault, reveal the style of fault evolution during the Pliocene-Quaternary, and establish plausible fault zone geometries in a region where many large Holocene earthquakes have terminated. In addition to these points, our detailed characterization of southern Alpine Fault geomorphology and shallow structure also provides a useful framework for future geodynamic or paleoseismic studies of the fault. The result of our work is a new perspective of the southern Alpine Fault that bears on neotectonics and earthquake hazards alike.

## 2. Background

The Alpine Fault is the ~850 km-long, active Pacific-Australian Plate boundary structure in the South Island of New Zealand (Figure 1; Norris & Cooper, 2001; Norris & Toy, 2014). The fault was initiated by the earliest Miocene as a primarily dextral structure (23 Ma, Cooper et al., 1987; Kamp, 1986), and was subsequently reorganized as a dextral-transpressive structure during the middle Miocene (c. 11-10 Ma, Cande & Stock, 2004; Lamb et al., 2015; Ring et al., 2019). Cumulative dextral strike-slip displacement on the central part of the fault has been argued to be 460–480 km (Hunt, 1978; P. R. King, 2000; Mortimer, 2014; Sutherland et al., 2000), or perhaps >700 km (Lamb & Mortimer, 2021; Lamb et al., 2016), depending on the assumed Eocene geometry of Zealandia's basement terranes.

The Alpine Fault is commonly divided into five sections based on geological characteristics and historic seismicity (Barth et al., 2013; references therein). Here we focus primarily on the southern section, although we also include parts of the central and Resolution sections in our analysis (Figure 1). These three fault sections have late Quaternary strike-slip rates of about 26–30 mm a<sup>-1</sup>, yet they exhibit different geomorphic, kinematic, and structural properties, and have generated different patterns of contemporary seismicity (Barnes, 2009; Barnes et al., 2001, 2005; Barth et al., 2012, 2013, 2014; Boese et al., 2012; Howarth et al., 2021; Langridge et al., 2014; Norris & Cooper, 2001, 2007; Warren-Smith et al., 2022).

The central section is generally the best-studied and understood. It is comprised of a localized (rather than distributed), northeast-striking (~055°) and moderately southeast-dipping (40–60°SE) fault plane that separates pelitic and psammitic schists of the Rakaia Terrane hanging wall from sandstone, mudstone, and greywacke of the Buller Terrane footwall (Cox & Barrell, 2007; Mortimer et al., 2013; Rattenbury et al., 2010; Toy et al., 2017). Geophysical imaging and thermal-kinematic modeling together suggest that the central Alpine Fault has a listric crustal geometry that soles into a subhorizontal décollement in the middle-lower crust of the Pacific Plate (Davey et al., 1995, 2007; Herman et al., 2009; Stern et al., 2007). Long-term dextral-reverse motion on this structure has driven hanging wall exhumation and topographic growth of the Southern Alps (Chamberlain et al., 1999; Herman et al., 2009). Late Cenozoic exhumation rates and magnitudes (Batt et al., 2000; Little et al., 2005; Tippett & Kamp, 1993) and late Quaternary fault-uplift and surface-uplift rates (Norris & Cooper, 2001; references therein) all feature maxima in the hanging wall near the middle of the central section and decrease southwest toward the southern section. The geomorphic expression of the fault zone along the central section appears localized, approximately linear, and geometrically simple only at large spatial scales (≥10 km). At the kilometer-scale,

MERE ET AL. 3 of 34

15252027, 2024, 11, Downloaded from https://agupubs.onlinelibrary.wiley.com/doi/10.1029/2024GC011839, Wiley Online Library on [12/03/2025]. See the Terms and Conditions

shallow strain is partitioned between juxtaposed dextral, dextral-reverse, and thrust segments; at the hundred meter-scale, dip-slip, strike-slip, and oblique-slip are partitioned across-strike into positive flower structures that root onto dextral and dextral-reverse segments (Barth et al., 2012; Langridge et al., 2014; Norris & Cooper, 1995, 1997; Upton et al., 2018). Major antithetic reverse faults are developed in the hanging wall, southeast of the central Alpine Fault trace due to bending of the overriding Pacific Plate (Cox et al., 2012; Little et al., 2005). Conversely, the Australian Plate footwall behaves approximately as a semi-rigid indenter (Batt et al., 2004; Kamp et al., 1992; Seward & Nathan, 1990) and it hosts no major active faults northwest of the central section (Langridge et al., 2016). On-fault background seismicity near the central Alpine Fault is low and the seismogenic zone is shallow; this reflects the locked nature of the fault and the high geothermal gradient due to long-term Pacific Plate exhumation, respectively (Boese et al., 2012; Leitner et al., 2001).

The southern Alpine Fault has been studied less than the central section, and differs from it both geometrically and kinematically. The fault plane is steep to subvertical rather than moderately dipping; surface geology and offshore geophysical imaging suggest an average dip of ~80°SE (Barnes et al., 2005; Barth et al., 2013). This steep dip leads us to favor sidewall, rather than hanging- and footwall, nomenclature. The geometry of the southern Alpine fault is poorly constrained and the relation between its steep surficial dip and crustal geometry is presently debated (cf., Howarth et al., 2021; Lamb et al., 2015; Warren-Smith et al., 2016, 2022). Slickensides developed on terrestrial fault plane exposures have subhorizontal rakes that indicate a dominance of dextral strike-slip with only a small component of relative footwall-up motion (~170°, Barth et al., 2013; Hull & Berryman, 1986; Sutherland & Norris, 1995). Seismic reflection and bathymetric imaging suggest similar kinematics offshore (Barnes et al., 2005). Both onshore and offshore, geomorphic fault expression has previously been described as linear and narrow (Berryman et al., 1992; Sutherland et al., 2006).

Basement geology, nearby structures, and seismicity also distinguish the southern from central section. Lithological variability is greater along the southern section than along the central section (Figure 1). This variability is greatest where ultramafics and sandstones of the Dun Mountain-Maitai Terrane, volcaniclastics of the Brook Street Terrane, and gneisses, schists, ultramafics, and diorites of the Tuhua Intrusives are juxtaposed in the eastern sidewall (Pacific Plate) by major faults inherited from earlier tectonic settings (Figure 1b). Previous work also details further lithological variability in the western sidewall of the southern Alpine Fault. Mapping by Barth et al. (2013) shows a narrow, ≥40 km long fault-parallel, serpentinite-bearing tectonic melangé along the southernmost onshore part of the fault, although earlier studies instead documented a shorter fault-truncated sliver of marine strata and granitic basement in a similar location (Nathan, 1978; Turnbull et al., 2010; Wellman & Wilson, 1964). Any late Tertiary-Quaternary motion on the major terrane-bounding faults in the eastern sidewall of the southern Alpine Fault is uncertain and poorly constrained. Nonetheless, patterns in contemporary seismicity suggest that some of these structures may accommodate the release of some plate boundary stress (Eberhart-Phillips et al., 2022; Warren-Smith et al., 2022). Microseismicity is also elevated on the northernmost ~20 km of the southern Alpine Fault, perhaps reflecting low on-fault frictional strength due to the local presence of partly serpentinized peridotites in the eastern sidewall (Figure 1b; Warren-Smith et al., 2022).

The offshore Resolution section ("rs" in Figure 1a) is perhaps the most structurally immature section of the Alpine Fault, based on its apparent age and structural connectivity of the principal zone of displacement. The boundary between the offshore southern section and the Resolution section is located offshore of Nancy Sound and is characterized by a 5–7 km wide, right-stepping (releasing) array of variable, yet steeply dipping fault segments that define a broad pull-apart structure and zone of distributed deformation (Barnes et al., 2005). A system of less active or Quaternary inactive faults extend southwest and approximately along-strike of the most landward segment of the Nancy pull-apart structure (Barnes et al., 2005; Lebrun et al., 2000). West-southwest of the pull-apart, the Resolution section appears segmented in bathymetric and seismic reflection imaging; it is composed of about three steeply southeast dipping fault segments that are each separated by right (releasing) steps and associated pull-apart basins (Barnes et al., 2001, 2005; Lebrun et al., 2000). This geometry reflects the localization of strike-slip deformation onto pre-existing rift faults in the Australian Plate that have been progressively juxtaposed against plate boundaries in the Pliocene-Quaternary (Lebrun et al., 2000). The southern end of the Resolution section terminates against the Puysegur trench, where the Australian Plate is obliquely subducted toward the east (Barnes et al., 2001, 2005; Lamarche & Lebrun, 2000; Lebrun et al., 2000).

MERE ET AL. 4 of 34

5252027, 2024, 11, Downloaded from https://agupubs.onlinelibrary.wiley.com/doi/10.1029/2024GC011839, Wiley Online Library on [12/03/2025]. See the Terms and Conditions

#### 3. Methods

#### 3.1. Topographic Data

For the purposes of geomorphic mapping and analysis, we utilized two data sets of high-resolution aerial lidar data. One data set was privately contracted by us for a 103 km-long Alpine Fault-parallel strip collected in 2016 and 2019, and the other was collected by the West Coast Regional Council near and northwest of the Alpine Fault (West Coast region) during the years of 2020–2022 (www.opentopography.com). All lidar data were processed using LAStools software following standard bare-earth point cloud processing workflows (https://lastools.github.io/). The bare-earth point clouds were triangulated and gridded as 1 m-resolution DEMs. To visualize the bare-earth topography and guide our geomorphic fault mapping, we utilized a combination of RGB composite hill-shade (Kokalj & Somrak, 2019), traditional hillshade, slope, and curvature models derived from the lidar DEMs. All spatial measurements subsequently reported are derived from the lidar data.

#### 3.2. Fault Zone Mapping and Analysis

Geomorphic fault expression reflects the interaction between earthquakes that create coseismic ground ruptures and surface processes that modify or otherwise remove evidence of these from the landscape. Within the footprint of our high-resolution topographic data, we mapped active fault traces, defined as a topographic lineament that corresponds to a surface or subsurface displacement discontinuity that is inferred to be tectonic in origin. Fault traces and their associated tectonic offsets are inferred to exist in the bare-earth topographic data where landforms are deformed or dissected, there are visible ruptures of the ground surface, erosional features are conspicuously linear and/or aligned, or where topographic lineaments cannot plausibly be attributed to other geomorphic or geologic features (e.g., stream gullies or terrace risers, glacial moraines, or foliation planes in bedrock). This methodology allows for mapping of shallowly and/or recently buried faults (e.g., post-1717 C.E. rupture of the central-southern Alpine Fault, Barnes et al., 2013; Berryman et al., 2012; De Pascale & Langridge, 2012; Howarth et al., 2021; Wells et al., 1999) and excludes mapping of deeply buried fault traces. Wherever possible, we validated our digital mapping against our field observations (Figure S1 in Supporting Information S1) and/or previously published observations and maps (Barth et al., 2013; Berryman et al., 1992; Rattenbury et al., 2010; Sutherland & Norris, 1995; Sutherland et al., 2006; Turnbull, 2000).

Our digital mapping workflow was as follows. First, we identified and mapped all apparent tectonic lineaments within our study area. Second, for each of these, we assigned a confidence ranking that ranged from certain, to likely, to probable. In assigning confidence rankings, we considered attributes such as magnitudes of apparent displacement, apparent fault trace length, apparent lineament azimuth, scarp topographic gradient, and scarp profile curvature (i.e., "topographic sharpness"), in addition to a qualitative assessment of the genetic ambiguity of each lineament. In the study area, we perceived genetic ambiguity in cases where apparent tectonic lineaments occur proximal to uphill-facing anti-slope scarps, both near ridgelines (Cotton et al., 1990; McCalpin, 1999; Ponti & Wells, 1991) and along foliation planes lower on the hillslopes (Beck, 1968; Bovis, 1982; Goodman & Bray, 1976), and also in cases where conspicuously linear erosional features occur near and subparallel to the regional fault network. Third, we interpreted each fault trace as either primary, subsidiary, or secondary. Primary fault traces are those we infer are connected to the principal zone of Alpine Fault displacement since at least the onset of regional deglaciation following the Last Glacial Maximum (18.3-17.4 ka; Barrell, 2011; Fink et al., 2006; Putnam et al., 2010, 2013). Subsidiary fault traces are those we infer are connected to fault planes other than the principal zone of displacement; we expect these to primarily accommodate patterns of distributed deformation. Secondary fault traces are those that are spatially correlated with, and hence, we infer are connected to, previously mapped faults other than the Alpine Fault. In the subsequent results and analysis we do not consider buried fault traces; we made this decision, in contrast to some previous studies (e.g., Khajavi et al., 2014; Vermeer et al., 2021), to limit uncertainty that may arise from errors in our interpretation of the landscape, and in light of the significant logistical challenge associated with visiting each and every mapped fault trace in our densely vegetated and remote study area.

Following digital mapping, we extracted the Cartesian coordinates and elevation values of the series of nodes on each fault trace. We fit a line to all points that define the Alpine Fault network and recorded the mean azimuth of these features. To record fault zone widths, we measured the distances perpendicular to this line between all points within the fault network within a 1 km sliding window (e.g., Manighetti et al., 2021). Using the three-dimensional data, we calculated best-fit planes for each system of points that defined a fault trace (e.g., Pearson, 1901). This

MERE ET AL. 5 of 34

15252027, 2024, 11, Downloaded from https

//agupubs.onlinelibrary.wiley.com/doi/10.1029/2024GC011839, Wiley Online Library on [12/03/2025]. See the Terms and Conditions (https://onlinelibrary.wiley.com/term

for rules of use; OA articles are governed by the applicable Creative Cor

method provides an accurate estimate of fault strike (0–179°) in cases where non-vertical planes intersect topography and yields an identical result to the mean fault trace azimuth if fault dip is subvertical to vertical. In ideal cases where fault planes intersect the Earth's free surface and topographic modification by off-fault deformation, erosion, or deposition is negligible, best-fit planes may be used to estimate fault dip (e.g., Thiele et al., 2017). We did not record model fault dip values, however, because these assumptions are rarely met within the study area, and additionally because fault dips may not be verified in-person for all but the most major, well-exposed fault strands. In addition to fault strike, we also calculated associated fault scarp aspects (0–359°) for each trace >50 m long based on the apparent senses of vertical surface displacement.

#### 3.3. Field Mapping

We mapped bedrock geology, where exposed, for  $\sim 10$  km along-strike and immediately northwest of the Alpine Fault between Lake McKerrow and to west of the Kaipo River (Figure 1b). To complement our fault trace mapping, we focused on constraining the lateral continuity of both bedrock faults and basement units.

In the field area, basement geology is obscured by late Quaternary fluvial, alluvial, glacial, and glacio-fluvial deposits (Barrell, 2011; Barth et al., 2014; Sutherland et al., 2007; Turnbull et al., 2010; Williams et al., 2015), thick soils (≥1 m, Almond & Tonkin, 1999), and dense podocarp-broadleaved and beech forest (Newsome, 1987). We therefore targeted basement outcrops revealed by active stream incision or recent hillslope failure (Korup, 2004; Norris et al., 1990). Extrapolation between these point observations allowed for the inference of map patterns, albeit with some uncertainty. We do not infer basement geology in large regions covered by Quaternary sediments, such as beneath major valleys or glacial plateaux.

#### 3.4. Zircon U-Pb Geochronology and Trace-Element Analysis

During field mapping, we collected representative whole-rock samples of several intrusive and/or metamorphic lithologies. We targeted these lithologies so that we could undertake petrochronological correlations based on mineralogical compositions and textures, zircon U-Pb age characteristics, and zircon trace-element compositions. We compare our data with previous petrochronological studies of the batholithic rocks in Zealandia to establish correlations (see Section 5.2).

Zircon grains were separated following standard heavy mineral separation procedures, were set into epoxy mounts, had equatorial cross sections exposed via grinding and polishing, and were imaged using both transmitted light and scanning electron microscope cathodoluminescence. The former imaging technique was used to identify included crystals, and the latter to image compositional zoning and internal grain morphology (e.g., Corfu et al., 2003; Hanchar & Miller, 1993; Rubatto & Gebauer, 2000; Schaltegger et al., 1999), and therefore, to guide the placement of laser ablation spots.

Zircon U-Pb isotopes and trace-elements were measured simultaneously via laser ablation split stream inductively coupled plasma mass spectrometry (LASS-ICP-MS) following the methods of Kylander-Clark et al. (2013). Isotope ratios were corrected using zircon 91500 (Wiedenbeck et al., 1995) as the primary reference material. Secondary reference materials Plešovice (Sláma et al., 2008), Temora 2 (Black et al., 2004), GJ-1 (Jackson et al., 2004), and AusZ5 (Kennedy et al., 2014) were used for quality control and yielded dates within 2% of their accepted values. Decay constants and the  $^{238}$ U/ $^{235}$ U ratio used are those of Jaffey et al. (1971) and Arden (1977), respectively. We calculated dates <1,400 Ma from  $^{206}$ Pb/ $^{238}$ U ratios that were corrected for common lead using the second-stage mantle reservoir model of Stacey & Kramers (1975) and the  $^{207}$ Pb/ $^{206}$ Pb correction method of Ludwig (2009). Dates >1,400 Ma are calculated from uncorrected  $^{207}$ Pb/ $^{206}$ Pb ratios. We infer that discordant dates reflect open-system behavior and we use these to calculate mixing-lines in  $^{207}$ Pb/ $^{206}$ Pb versus  $^{238}$ U/ $^{206}$ Pb space that constrain the timing of open-system events (e.g., Tera & Wasserburg, 1972). Zircon core ages that are  $\geq$ 400 Ma and  $\geq$ 90% concordant are used to construct inherited age spectra (e.g., Adams et al., 2015). All U-Pb dates are reported at the  $2\sigma$  uncertainty level.

#### 4. Results

## 4.1. Geomorphic Fault Mapping

The central Alpine Fault manifests as a linear feature along the southern Haast coastal plain and in the Jackson River valley (Figure 2a). Fault traces are inferred primarily where alluvial fan and fluvial overbank deposits are

MERE ET AL. 6 of 34

1250E

1.525207, 2024, 11, Dowloaded from https://apupubs.onlinelibary.wiley.com/doi/10.1029/2024GC011839, Wiley Online Library on [12/032025]. See the Terms and Conditions (https://onlinelibary.wiley.com/terms-and-conditions) on Wiley Online Library for rules of use; OA articles are governed by the applicable Creative Commons Licenson

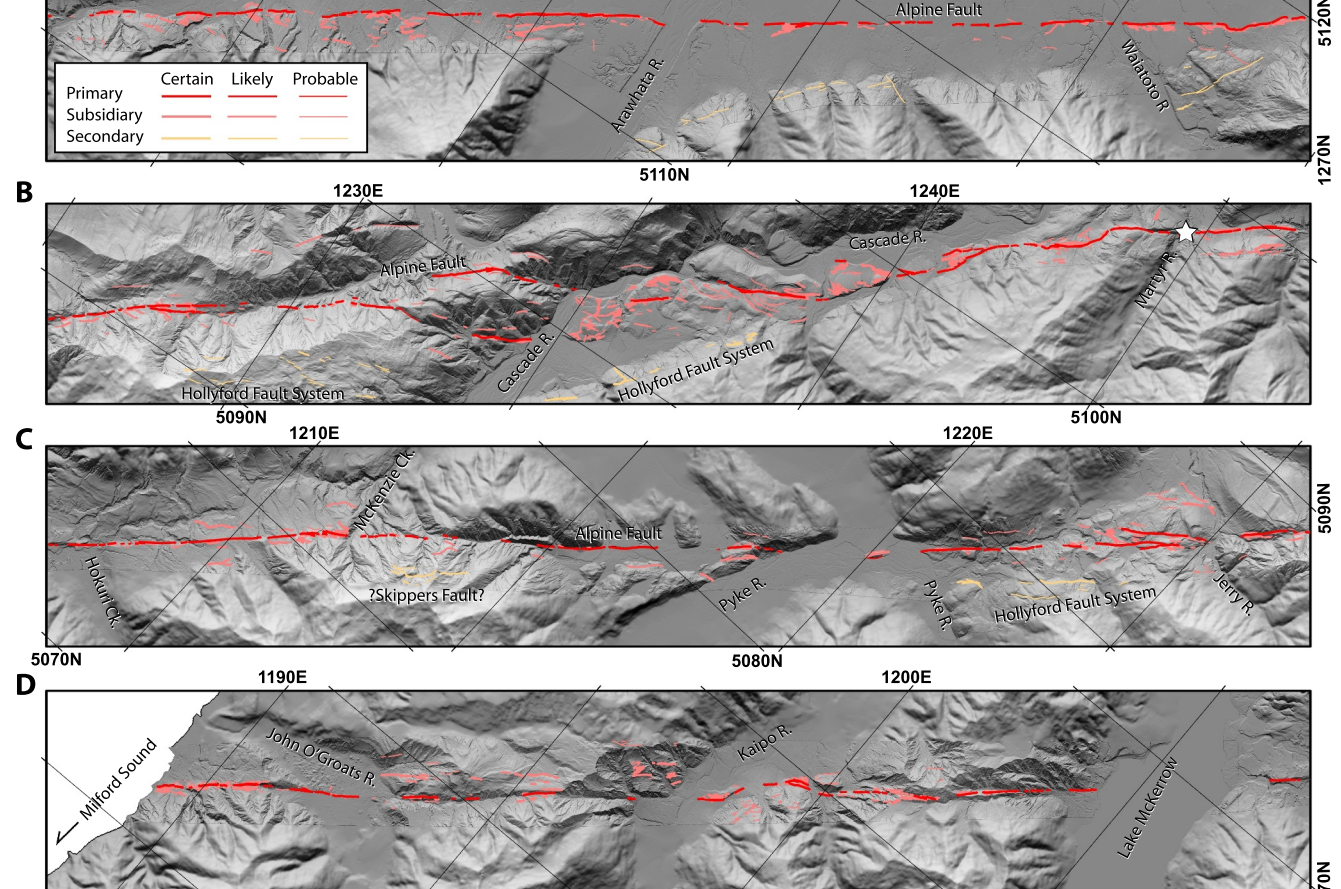


Figure 2. (a) Fault trace maps of the central and (b)–(d) southern onshore sections of the Alpine Fault and associated secondary faults. Panels are arranged from northeast to southwest. White star depicts the central-southern section boundary. A description of fault zone morphology is provided in the text. Reference grid easting and northing values are displayed in kilometers and are derived from the New Zealand Geodetic Datum 2000. Note the slight anticlockwise rotation of the reference frame between panels (a)–(b) and (c)–(d). Digital elevation and hillshade models within and outside of the Alpine Fault Zone are lidar-derived (this study) and sourced from regional topographic maps derived from stereo-paired aerial photography (www.otago.ac.nz/surveying/research/geospatial/digital-elevation-model), respectively.

uplifted to the southeast and dextrally offset by fault motion. Geomorphic fault expression is laterally continuous except where the fault is buried by recent sedimentation or it traverses active fluvial channels. Subsidiary fault traces occur almost exclusively in the hanging wall. Near the Jackson River, fault traces bound an elongated fault-parallel zone of uplift. Probable secondary fault traces are evident where bedrock hillslopes and landslide deposits are offset immediately north of the Arawhata River and Waiatoto River; these record apparent northwest-up and dextral motion and have geometries that curve southwards away from their intersections with the Alpine Fault.

1260E

The surface expression of the southern Alpine Fault is variable and more complex than along the central section. Fault traces are evident where they offset and/or deform bedrock hillslopes, ridges, alluvial fans, fluvial overbanks, and glacial deposits (Figures 2b–2d). Primary fault traces commonly record large-magnitude ( $10^2$  to  $10^3$  m-scale) dextral displacements in addition to a subordinate component of northwest-up motion. A striking feature of the fault zone is an arrangement of multiple primary fault traces in the Cascade River valley, immediately south of the central-southern section boundary (Figure 2b), some of which were previously identified by Berryman et al. (1992). Here, three to four left-stepping and overlapping en-echelon primary fault traces traverse a northwest (releasing) stepover in the fault zone (Figure 2b). Farther to the southwest, primary fault traces are comparatively linear and localized; most apparent complexity in geomorphic expression results from distributed subsidiary faulting (Figures 2c and 2d). These subsidiary fault traces occur in both the eastern and western sidewalls. Apparent oblique dextral and northwest-up displacements ( $10^0$  to  $10^1$  m-scale) are commonly associated with

MERE ET AL. 7 of 34



these subsidiary fault traces. We map a few anomalous southeast-up fault traces with little evidence of apparent dextral displacement in the western sidewall between the Cascade River valley and southern coastline (Figures 2c and 2d). We infer secondary fault traces where they offset hillslopes in the eastern sidewall of the Alpine Fault. These bifurcate southwards from the Alpine Fault in the Cascade River valley and extend subparallel to the fault at least as far southwest as near McKenzie Creek.

We summarize morphological parameters to reveal systematic patterns, or lack thereof, along the length of the Alpine Fault. Topography within 1 km perpendicular to the primary fault trace ranges from  $\sim$ 0 to 1,140 m (Figure 3a). Near-fault topography is only slightly asymmetric along most of the fault, with elevation in the hanging wall or eastern sidewall typically exceeding that in the footwall or western sidewall by <200 m. The regions of greatest topographic asymmetry feature elevations that are  $\sim$ 400–500 m greater in the eastern sidewall of the Alpine Fault (e.g., near McKenzie Creek and the northernmost Cascade River valley,  $\sim$ 25–32 km and  $\sim$ 65–72 km distance in Figure 3a).

In the study area, the width of the Alpine Fault Zone is highly variable. Primary fault traces define a narrow zone of deformation along both sections that is interrupted only by the 1.5-km-wide stepover and en-echelon trace arrangement in the Cascade River valley. Conversely, the zone of primary *and* subsidiary fault traces is both wider and displays much greater spatial variability. Including these traces, fault zone width ranges from <100 m to >1,700 m, and is notably elevated (almost exclusively  $\geq$ 0.5 km-wide) along the southern section and along the southernmost part of the central section in the Jackson River valley (Figure 3b).

Fault strikes are variable within the study region. Subsidiary and secondary fault traces contribute disproportionately to this scatter because they exhibit about two times greater variance in strike than primary fault traces (Figure 3b). There is a clear spatial correlation between the variance of fault strikes and fault zone width (Figure 3b). Including subsidiary fault traces, the zone of greatest width (~1.5 km-wide) and geometric complexity extends from the Cascade River to the Jerry River. Linear regression of certain and likely primary fault traces reveals mean fault zone azimuths of 58° between the Waiatoto River and Martyr River (25 km-long, central section), 49° between the Jerry River and Lake McKerrow (25 km-long, southern section), and 53° between Lake McKerrow and the southern coastline (limited to 21 km-long, southern section; Figure 3b).

Length-weighted rose diagrams of fault strikes reveal similar central tendencies of  $50\text{--}60^\circ$  between the three above cited populations of fault traces, though dissimilar azimuthal distributions (Figure 3c). Primary fault planes exhibit strikes mostly between  $\sim$ 45 and  $60^\circ$ . Subsidiary fault planes feature a broader distribution between  $\sim$ 45 and  $75^\circ$ . Secondary fault planes exhibit two distinct peaks, between  $\sim$ 25 and  $35^\circ$  and  $\sim$ 45– $60^\circ$ . The azimuthal distribution of secondary fault planes reflects regions of bifurcation between these and the Alpine Fault Zone (Figure 2).

We infer that fault scarp aspects proxy the dip-slip component of fault motion. These are dominantly northwest-facing on the central section, and dominantly southeast-facing on the southern section of the Alpine Fault (Figure 3d). This pattern corroborates our previously discussed qualitative assessment of apparent vertical displacements. Topographic profiling and topographic visualizations both show that the along-strike pattern, from northwest to southeast facing scarps, is associated with a change in scarp morphology, from rounded (lower topographic curvature) on the central section to sharp (higher topographic curvature) on the southern section. We infer that finer-scale patterns developed in scarp aspects reflect local variability in the orientation and/or dip-slip component of motion on subsidiary fault planes.

#### 4.2. Geologic Mapping

Our field investigation reveals a slice of fault-bound basement units immediately northwest of the principal strand of the Alpine Fault (Figure 4a). This material is distinct in that it locally disrupts the juxtaposition of the Greenland Group metasandstone of the Buller Terrane (Mortimer et al., 2013) to the north and the St. Anne Gneiss of the Tuhua Intrusives (Wood, 1972) to the south of the fault, respectively. By outcrop area, basement units include complexly folded calcareous marine sediments, several granitic to metagranitic lithologies, and an intensely fractured and hydrothermally altered band of quartzofeldspathic to micaceous rock that we characterize as the Alpine Fault damage zone (~100 m-wide, Figure 4b). Comparison between our field and petrographic notes (Text S1 in Supporting Information S1) and previous work supports correlation between the calcareous sedimentary units exposed within the Alpine Fault Zone and the Tititira Formation (and/or the Jackson

MERE ET AL. 8 of 34

15252027, 2024, 1, Downloaded from https://agupubs.online1brary.witey.com/doi/10.1029/2024GC011839, Wiley Online Library on [12/032025]. See the Terms and Conditions (https://onlinelbbrary.witey.com/terms-and-conditions) on Wiley Online Library for rules of use; OA articles are governed by the applicable Creative Commons Licenseauch

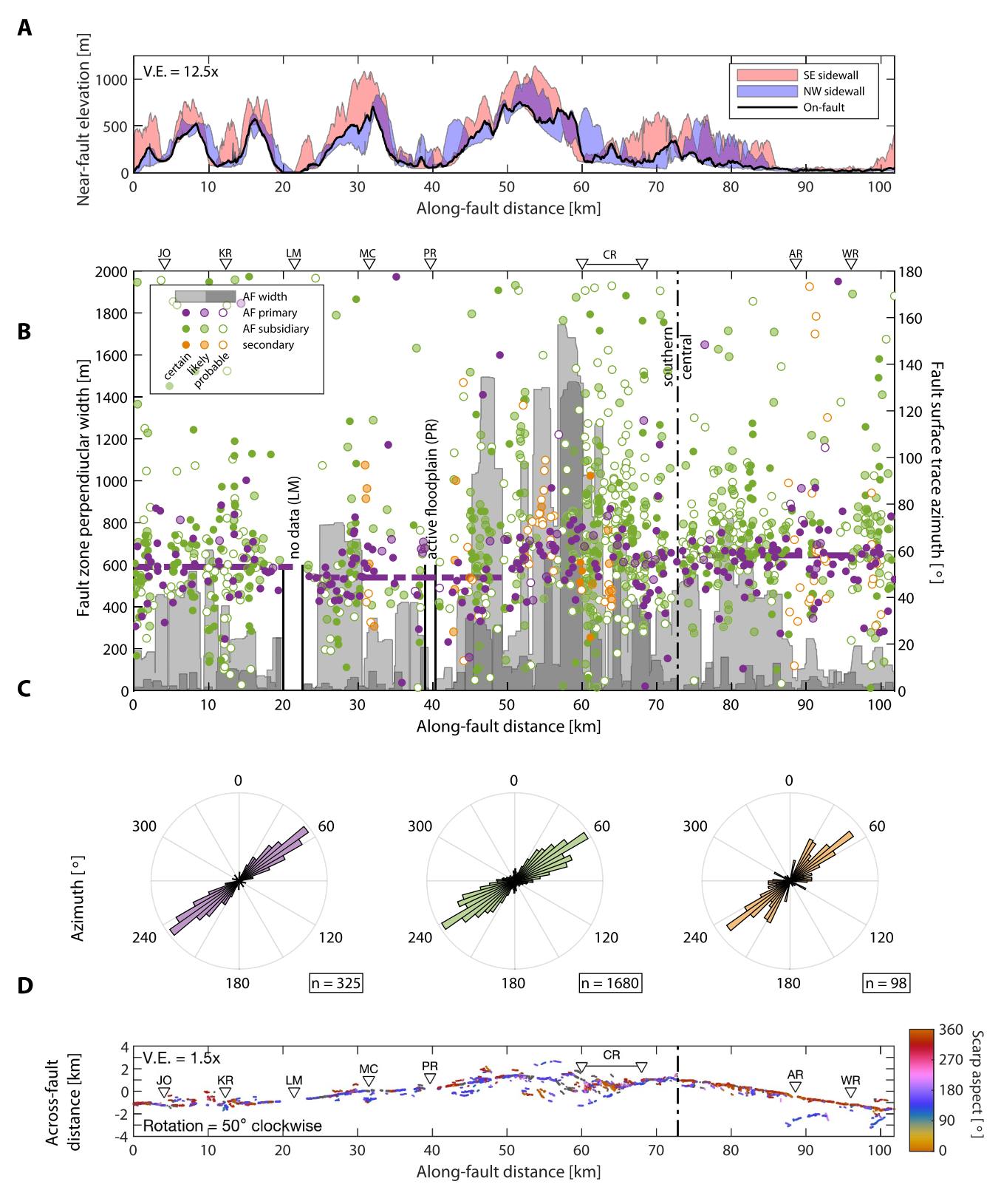


Figure 3.

MERE ET AL. 9 of 34

15252027, 2024, 11, Downloaded from https://agupubs.onlinelibrary.wiley.com/doi/10.1029/2024GC011839, Wiley Online Library on [12/03/2025]. See the Terms and Conditions

(https://onlinelibrary.wiley.com/terms-and-conditions) on Wiley Online Library for rules of use; OA articles are governed by the applicable Creative Commons Licensu

Formation, which occurs as a series of allochthonous bodies within the former) that is exposed  $\sim$ 6 km to the northwest along the coast (Nathan, 1978; Sutherland et al., 1996). Conversely, crystalline basement exhibits greater lithological variability than has previously been recognized. Shear, brittle fracture, and hydrothermal alteration overprints are all preferentially developed to the northwest of the Alpine Fault, and these increase in development with proximity to the fault (Text S1 in Supporting Information S1).

At least three fault-bound slivers of crystalline basement are in-faulted into the center of the wider slice of the Tititira Formation (Figure 4a). The northwestern sliver is composed predominantly of biotite-muscovite granodiorite, which intrudes into a subordinate amount of microdiorite. This field relationship is particularly clear where deformed granodiorite dikes intrude into the microdiorite; elsewhere, we observed an irregular intrusive contact between the two lithologies. The central sliver is composed of monzogranite that exhibits crude gneissic banding in the vast majority of outcrops. The southeastern sliver is small and composed of monzogranite that is intruded by microdiorite. We observe this field relationship where small (10<sup>-1</sup> m-scale) dikes and enclaves of microdiorite are present in monzogranite. The relative proportion of these lithologies is challenging to assess given the sparse frequency of outcrops. In Section 4.3 and 5.1, we focus on the zircon U-Pb characteristics and petrography of these crystalline basement units, and we present data that may be used to evaluate possible correlations, including a previously hypothesized correlation to the Karamea Suite, similar to other granitic bodies mapped nearby in the Buller Terrane (Tulloch et al., 2009; Turnbull, 2000, references therein).

The geometry of the Alpine Fault Zone can be inferred from combined geologic-geomorphic mapping (Figures 2 and 4a). These maps show that many of the unit-bounding bedrock faults we mapped in the field are aligned along-strike of those expressed in the bare-earth topographic data. Outcrop observations demonstrate the lateral continuity of both basement units and their bounding faults. Together, these relationships imply greater fault lengths than does geomorphic fault expression alone. We therefore infer connectivity of the faults within the fault zone.

The Alpine Fault Zone is bounded to the northwest by a very steep southeast-dipping fault that we observe in bedrock outcrops and term the northwestern strand (Figure 4). The northwestern strand exhibits subtle geomorphic expression along most of its length (Figure 2d). Therefore, we constrain its position not only by connecting geomorphic and geologic fault traces but also by using the lateral continuity of Tititira Formation outcrops. In this way, our mapping and that of Turnbull (2000) show that outcrops of the Tititira Formation occur at least between the John O'Groats River and Lake McKerrow. Furthermore, Barth et al. (2013) identified distinct basement units within the Alpine Fault Zone that include deformed correlatives of the calcareous sedimentary units exposed in the Kaipo Slips (in addition to altered granitoids) at both Hokuri and McKenzie Creek. Synthesis of new and existing data therefore shows that the northwestern strand bifurcates from the principal strand of the Alpine Fault near the John O'Groats River and is continuous at least as far north as Hokuri Creek (~22 km) and perhaps as far north as McKenzie Creek (~28 km).

We observe a network of faults in bedrock outcrops that extend along the central axis of the Alpine Fault Zone in the field area (Figure 4). These faults are subparallel, northeast-striking, and steeply northwest-dipping ( $>60^{\circ}$ ). West of the Kaipo River, these subparallel faults are linked in places by shorter, more northerly striking and curvilinear faults. Together, these faults within the central axis of the Alpine Fault Zone bound the previously discussed crystalline basement slivers. Consistent with both field and geomorphic observations, we infer that these faults tend to bifurcate and/or merge into each other at distance along-strike (Figure 4a). This characteristic is particularly evident where these faults dissect or deform late Quaternary glacial deposits. On the other hand, we are less certain of their along-strike continuity where they are covered by Holocene alluvium in the Kaipo River Valley (Figures 2d and 4a). Extrapolation of surface fault dips to depth shows two important characteristics. First, if we consider that the faults that bound the crystalline basement slivers are roughly planar, linear projections of these imply they splay from the northwestern strand at shallow depths ( $\sim$ 0.5–1 km). The precise depth of this bifurcation is dependent on which faults truncate others, which is uncertain given the presently available data.

**Figure 3.** Summary of fault zone geomorphology and structure. (a) Near-fault topography. Elevation values are extracted within 1-km wide fault-parallel swaths centered in the southeastern and northwestern sidewalls of the Alpine Fault. (b) Fault zone perpendicular width and fault plane strikes (0–179°). Dark and light shaded regions show fault zone width measured using only primary, and primary plus subsidiary fault traces, respectively. Dashed lines show mean fault zone azimuths described in the text. (c) Length-weighted rose diagrams of fault strikes, color coded as in the previous panel. (d) Fault scarp aspects. AR, Arawhata River; CR, Cascade River; JO, John O'Groats River; KR, Kaipo River; LM, Lake McKerrow; MC, McKenzie Creek; PR, Pyke River; WR, Waiatoto River; V.E., Vertical Exaggeration.

MERE ET AL. 10 of 34

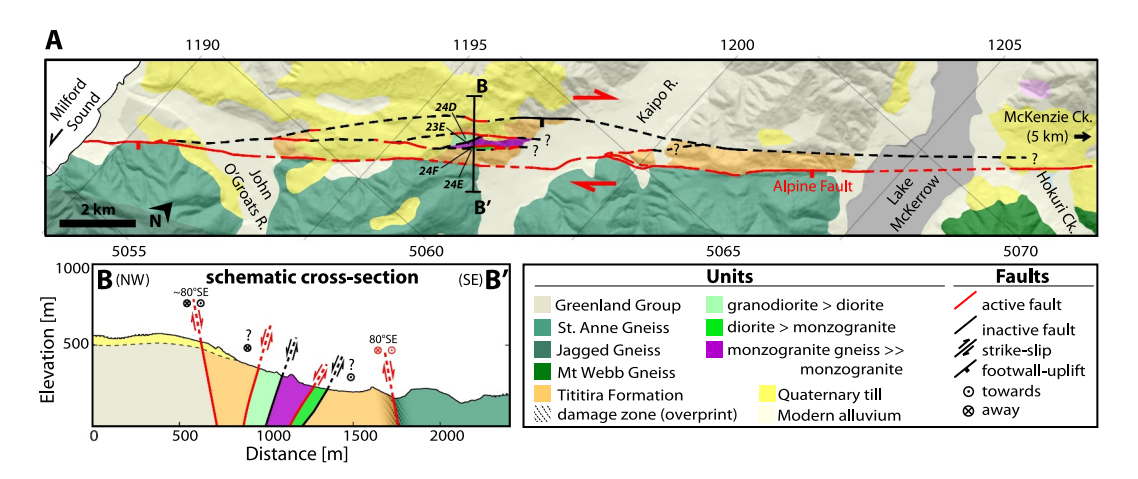


**Figure 4.** Results of combined geologic-geomorphic mapping. (a) Geologic map of the field area. The Alpine Fault Zone is notably wide and is cored by basement lithologies that are not found elsewhere within the fault zone. The spatial distributions of geologic units are based on the integration of our mapping with previously published maps of Turnbull (2000) and Barth et al. (2013). Easting (top) and northing (bottom) values are shown in kilometers. (b) Schematic geologic cross-section.

Second, steep dips of both the Alpine Fault and the northwestern strand imply that if these two faults merge, this must occur at much greater depth, even if one or both of these structures are non-planar.

#### 4.3. Geochronology of Granitic Units

As previously stated, we identified at least four different granitic lithologies in basement fault slivers northwest of the Alpine Fault near the Kaipo Valley. Here, we present the zircon U-Pb geochronology results of these units. Petrographic and geochronological summaries are provided in Table 1.

#### 4.3.1. Biotite-Muscovite Granodiorite (24D)

Zircon forms colorless to pink euhedral crystals. Cathodoluminescence imaging revealed a core-rim structure in 73% of zircon grains (Figure 5a). Cores exhibit diverse internal zoning patterns and commonly irregular resorbed morphologies. Rim domains exclusively exhibit oscillatory zoning, as do zircon crystals lacking core-rim structure (single-grains).

Ninety-nine spot analyses of forty-five zircon crystals yield predominantly Early Cretaceous  $^{206}\text{Pb}/^{238}\text{U}$  dates in addition to scattered Paleozoic-Proterozoic dates. Of the Early Cretaceous analyses, single-grains notably compose two distinct clusters of dates that are separated by >6 Ma and that do not overlap within error. We use the analyses that compose these clusters to calculate error-weighted mean ages, excluding discordant analyses, of  $111.9 \pm 2.2$  Ma (n = 15, MSWD = 2.30) and  $121.1 \pm 2.4$  Ma (n = 4, MSWD = 0.70; Figure 5b). Zircon cores record this latter age component; these yield a statistically indistinguishable error-weighted mean age of  $120.4 \pm 2.2$  Ma (n = 6, MSWD = 0.45; Figure 5b). Zircon rim dates range between 110 and 132 Ma in addition to some scattered Jurassic-Proterozoic dates. The inherited age spectrum features a prominent mode at c. 525 Ma.

#### 4.3.2. Biotite-Hornblende Diorite (23F)

Zircon forms small ( $\sim$ <100 µm long), colorless to pink, euhedral-subhedral crystals, many of which are fragmented. Cathodoluminescence imaging shows that zircon crystals exhibit continuous growth zoning (Figure 5c); one crystal exhibits an apparent core-rim structure.

Sixteen spot analyses of ten zircon grains yield  $^{206}\text{Pb}/^{238}\text{U}$  dates that are predominantly clustered in the Cretaceous and Jurassic. These clusters describe two steeply discordant arrays in the Tera-Wasserburg space that imply Pb contamination from a reservoir of high  $^{207}\text{Pb}/^{206}\text{Pb}$  (Figure 5d). Because the common Pb value is well described by each discordia array, we use the common Pb corrected  $^{206}\text{Pb}/^{238}\text{U}$  dates to calculate an errorweighted ages of  $120.7 \pm 2.4$  Ma (n = 6, MSWD = 1.7) and  $164.1 \pm 5.8$  (n = 5, MSWD = 8.4, Figure 5d, inset). The younger of these ages is statistically indistinguishable from a lower-intercept discordia age of

MERE ET AL. 11 of 34

15252027, 2024, 11, Downloaded from https://agupubs.onlinelibrary.wiley.com/doi/10.1029/2024GC011839, Wiley Online Library on [12/032025]. See the Terms and Conditions (https://onlinelibrary.wiley.com/terms-and-conditions) on Wiley Online Library for rules of use; OA articles are governed by the applicable Creative Commons. Licensea

 Table 1

 Summary of Petrochronological Data From This Study

Note. All zircon U-Pb ages are reported in Ma at the 2 $\sigma$ -uncertainty level unless reported as approximate (c.). Mineral abbreviations follow Whitney and Evans (2010): Aln, alanite; Ap, apatite; Bt, biotite; Chl, chlorite; Ep, epidote; Hbl, hornblende; Msc, muscovite; Ser, sericite; Tn, titanite; Zrn, zircon.

15232027, 2024, 11, Dewloaded from https://agupub.co.nline1brary.witey.com/doi/10.1029/2024GC011839, Wiley Online Library on [12/032025]. See the Terms and Conditions (https://onlinelbrary.witey.com/terms-and-conditions) on Wiley Online Library for rules of use; OA articles are governed by the applicable Creative Commons Licenseauch

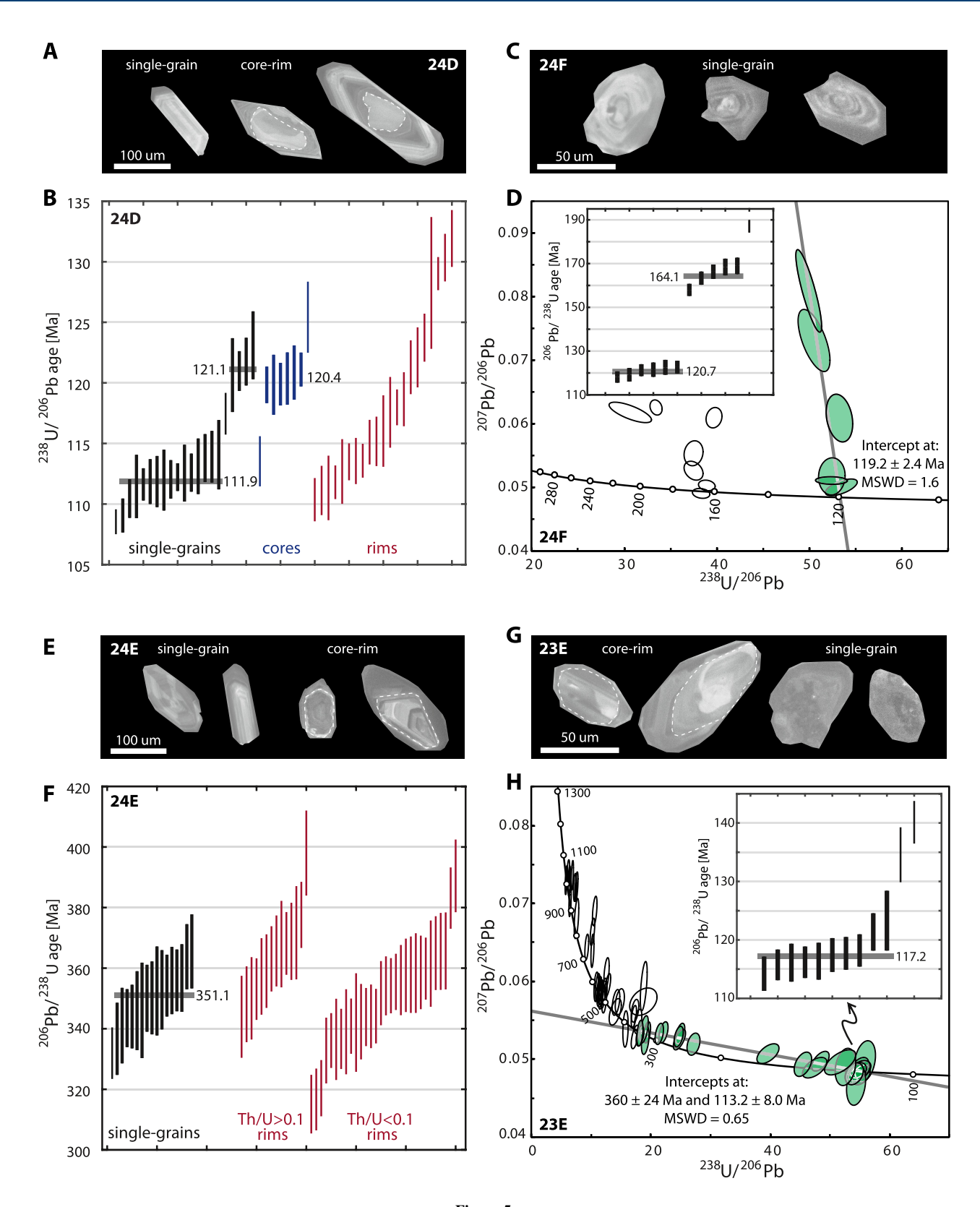


Figure 5.

MERE ET AL. 13 of 34

5252027, 2024, 11, Downloaded from https://agupubs.onlinelibrary.wiley.com/doi/10.1029/2024GC011839, Wiley Online Library on [12/03/2025]. See the Terms and Conditions

(https://onlinelibrary.wiley.com/terms-and-conditions) on Wiley Online Library for rules of use; OA articles are governed by the applicable Creative Commons Licensu

 $119.2 \pm 2.4$  Ma (n = 6, MSWD = 1.6) calculated using the younger cluster of dates. We regard a single, highly discordant date of 93.5 Ma to reflect Pb-loss and two Neoproterozoic ages to reflect inheritance.

#### 4.3.3. Biotite Monzogranite (24E)

Zircon forms colorless, euhedral crystals. Cathodoluminescence imaging reveals core-rim structure in 81% of grains. Cores exhibit diverse zoning patterns and commonly exhibit resorption textures. Rims characteristically exhibit weak oscillatory zoning. Single-grain zircon features continuous growth patterns including concentric oscillatory and sector zoning and is smaller than grains with core-rim structure (Figure 5e).

One-hundred-and-twenty-seven spot analysis of forty zircon grains yields predominantly Devonian-Carboniferous  $^{206}$ Pb/ $^{238}$ U dates in addition to scattered early Paleozoic-Proterozoic dates. Segregation of these analyses by zircon domain shows that single-grains yield the most narrow distribution of dates that are clustered in the early Carboniferous. Accordingly, we used these single-grain analyses to calculate an error-weighted mean age of 351.1  $\pm$  7.0 Ma (n = 16, MSWD = 1.90). Rim analyses yield a multimodal distribution of dates that is suggestive of multiple possible components. Of these, >70% yield Th/U <0.10. Considering only those rims with Th/U >0.10 reveals a more restricted distribution of dates that ranges between 348 and 378 Ma (Figure 5f). Cores characteristically yield the oldest U-Pb dates and are predominantly >400 Ma. The inherited date spectrum features prominent modes at c. 550 Ma, c. 630 Ma, and c. 490 Ma. We infer that a single discordant Jurassic date reflects Pb-loss.

#### 4.3.4. Monzogranite Gneiss (23E)

Zircon forms colorless, subhedral-euhedral crystals. Cathodoluminescence imaging reveals core-rim structure in 80% of these. Cores exhibit diverse zoning patterns including oscillatory, banded, and convolute zoning. Rim domains show oscillatory zoning that is commonly blurred. Single-grain crystals tend to exhibit convolute or patchy zoning and notably weaker cathodoluminescence response (Figure 5g).

Sixty-seven spot analyses of thirty-seven zircon crystals yield variably concordant  $^{206}\text{Pb}/^{238}\text{U}$  dates that range between the Early Cretaceous and Proterozoic. Plotting these analyses in the Tera-Wasserburg space suggests multiple apparent mixing lines; however, these are primarily composed of analyses with corrected  $^{206}\text{Pb}/^{238}\text{U}$  dates >350 Ma (Figure 5h). Analyses younger than this age describe a single mixing line between the middle Paleozoic and Early Cretaceous and correspond predominantly to low Th/U ( $\leq$ 0.10) zircon that exhibit convolute or blurred oscillatory zoning. We used these data, excluding two highly discordant analyses that significantly reduced model goodness-of-fit, to calculate upper- and lower-intercept discordia ages of  $360 \pm 25$  Ma and  $113.2 \pm 8.2$  (n = 25, MSWD = 0.65, Figure 5h), respectively. This lower-intercept age is statistically indistinguishable from an error-weighted mean age of  $117.2 \pm 2.3$  (n = 10, MSWD = 2.2) calculated using only concordant analyses within the Early Cretaceous cluster (Figure 5h, inset). The inherited date spectrum features a prominent mode at c. 522 Ma. We infer that one anomalously young grain (c. 87 Ma) is affected by Pb-loss.

#### 4.4. Zircon Trace-Element Data

Trace element data including Hf concentrations, U/Yb, Ce/Yb, and Gd/Yb ratios that correspond to laser ablation analyses of Jurassic or Cretaceous aged zircon from samples 24D and 24F are shown in Figure 6, which shows the chemical similarity of zircon from these samples. Hf concentrations range between  $\sim$ 7,000 and 19,000 ppm (24D) and  $\sim$ 9,000–12,000 (24F), U/Yb ratios range between 0.3 and 4.5 (24D) and 0.4–1.5 (24F), Ce/Yb ratios range between 0.001 and 1 (24D) and 0.02–0.1 (24F), and Gd/Yb ratios range between 0.008 and 0.3 (24D) and 0.04–0.1 (24F). The significance of these chemical similarities are discussed in Section 5.2.

Figure 5. Summary of zircon cathodoluminescence and LA-ICP-MS U-Pb geochronology. (a), (c) First and (e), (g) third rows show representative example cathodoluminescence images of analyzed zircon crystals. Labels denote identified subpopulations based on internal crystal morphology. Dashed thin lines depict inferred boundaries between core and rim domains. (b), (d) Second and (f), (h) fourth rows show the results of LA-ICP-MS U-Pb geochronology, predominantly for analyses with corrected  $^{206}\text{Pb}/^{238}\text{U}$  ages <400 Ma. Age plots are presented as either error-weighted means (b), (f) or discordia arrays with ages labeled in Ma (d), (h) based on U-Pb characteristics of the respective sample. All error bars and error ellipses depict  $2\sigma$  uncertainties. Filled and open ellipses are used and not used for discordia regressions, respectively.

MERE ET AL. 14 of 34

15252027, 2024, 11, Downloaded from https://agupubs.onlinelibrary.wiley.com/doi/10.1029/2024GC011839, Wiley Online Library on [12/03/2025]. See the Terms and Conditions (https://onlinelibrary.

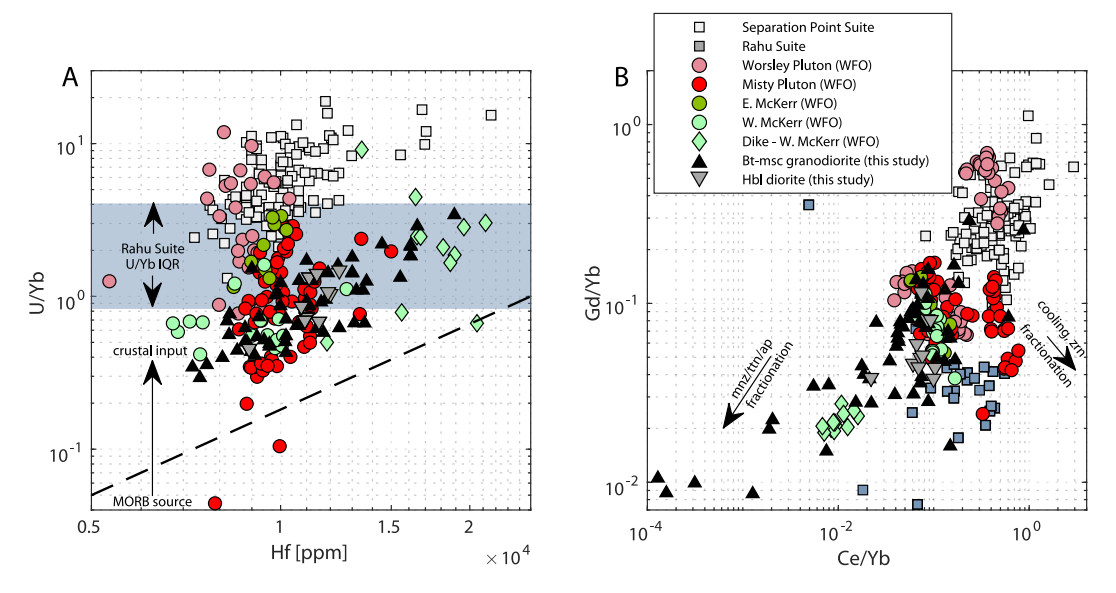


**Figure 6.** Zircon trace-element analyses. (a) U/Yb versus Hf. (b) Gd/Yb versus Ce/Yb. In both plots, note that zircon from the Cretaceous diorite and granodiorite units that we map within the Alpine Fault Zone in the study area display the greatest overlap with the Western McKerr Intrusives and related post-kinematic dike (Schwartz et al., 2017). Arrows in both plots depict geochemical evolution trajectories, given the occurrence of the labeled phenomenon (Grimes et al., 2015). Hf concentration data are not available for the Rahu Suite and hence the interquartile range (IQR) of U/Yb ratios is shown for reference. WFO, Western Fiordland Orthogneiss; MORB, Mid-ocean ridge basalt; ap, apatite; mnz, monzanite; ttn-titanite; zrn-zircon.

#### 5. Petrochronological Interpretations

#### 5.1. Timings of Granitoid Emplacement and Metamorphism

Here we provide our interpretations of the zircon U-Pb geochronology results, and hence justify the magmatic emplacement, metamorphic, and inherited age components listed in Table 1.

The muscovite monzogranite (24E) was emplaced at  $351.1 \pm 7.0$  Ma. This age is recorded by euhedral, oscillatory zoned, high Th/U (>>0.10), single-grain zircon. These characteristics support an Early Carboniferous emplacement age because they are indicative of zircon grown in a parent melt (Corfu et al., 2003; Hanchar & Miller, 1993; Hoskin & Ireland, 2000; Rubatto & Gebauer, 2000).

The monzogranite gneiss (23E) protolith was emplaced at  $360 \pm 25$  Ma, and metamorphism occurred at  $117.2 \pm 2.3$  Ma. These ages are supported by an Early Cretaceous-Early Carboniferous mixing line that is suggestive of open-system behavior. The younger age of metamorphism is supported by low Th/U ( $\leq$ 0.10) analyses of single-grains and rims that exhibit convolute or blurred oscillatory zoning. These isotopic and textural characteristics are consistent with trace-element redistribution coeval with metamorphic zircon recrystallization (Connelly, 2001; Corfu et al., 2003; Hoskin & Black, 2000; Rubatto, 2017; Schaltegger et al., 1999; Yakymchuk et al., 2018). The upper-intercept discordia age of emplacement is imprecise. Nonetheless, given the similarity in petrography and emplacement age (Table 1), we infer that both monzogranitic lithologies are correlated.

The biotite-hornblende diorite was emplaced at  $120.7 \pm 2.4$  Ma and inherited zircon that contained a c. 164 Ma age component. This inference is supported by Early Cretaceous zircon with internal zoning characteristics and Th/U that are suggestive of magmatic growth. Mineral assemblages within the biotite-hornblende diorite suggest a maximum of greenschist-facies alteration (orthopyroxene, clinopyroxene, and garnet are notably absent, Table 1). Zircon grown under greenschist-facies conditions has distinctive characteristics that we do not observe (Dempster et al., 2004; Hay & Dempster, 2009; Rubatto, 2017). Therefore, an alternative hypothesis that the younger age reflects the timing of a metamorphic event is not supported by the data. Although zircon inheritance may be limited in some mafic rocks due to high zircon solubility in the parent magmas (Watson, 1979; Watson & Harrison, 1983), inherited zircons have been documented in many previous studies of mafic granitoids (Bea

MERE ET AL. 15 of 34

15252027, 2024, 11, Downloaded from https://agupubs

online library wiley com/doi/10.1029/2024GC011839, Wiley Online Library on [12/03/2025]. See the Terms and Conditions

et al., 2020, references therein), including those elsewhere in New Zealand (Bhattacharya et al., 2018; Schwartz et al., 2017, 2021; Tulloch et al., 2011; Turnbull et al., 2013).

The biotite-muscovite granodiorite was emplaced at  $111.9 \pm 2.2$  Ma and inherited zircon that contained a  $120.4 \pm 2.2$  Ma age component. The Early Cretaceous emplacement age is recorded in euhedral single-grain zircon that exhibit oscillatory zoning and high Th/U (>>0.10). Conversely, the older Early Cretaceous age manifests primarily in oscillatory zoned high Th/U cores that are overgrown by younger, c. 112 Ma rims. These characteristics support our interpretations of both the emplacement and inherited age components (Corfu et al., 2003; Hanchar & Miller, 1993; Hoskin & Ireland, 2000; Rubatto & Gebauer, 2000). Considering intrusive field relationships and statistically indistinguishable  $Pb^{206}/U^{238}$  ages, we infer that the inherited zircon was sourced from the 119.7 Ma hornblende microdiorite.

#### 5.2. Petrochronological Correlations

The fault-bounded slivers of crystalline basement that crop out northwest of the southern Alpine Fault are not derived from a single intrusive suite, as may be the case for nearby granitic intrusions within the Buller Terrane (Rattenbury et al., 2010). Instead, they are likely fragments of bedrock rock that have been displaced by the Alpine Fault. In the South Island, plutonic and hypabyssal basements are encompassed by the Tuhua Intrusives component of the Western Province (Mortimer et al., 2014). Because the Tuhua Intrusives have been dismembered by Cenozoic motion on the Alpine Fault (Figure 1a), they represent a likely source of the allochthonous basement slivers. Here we consider correlations between these units and suites (or plutons) within the Tuhua Intrusives because this may provide new constraints on the slip history of the southern Alpine Fault.

The Tuhua Intrusives intersect the Alpine Fault in the northern (Nelson block, Kimbrough et al., 1993; Tulloch & Kimbrough, 1989) and southern parts of the South Island (Fiordland block, Oliver & Coggon, 1979; Figure 1a). Displacement of the basement slivers from the north block is unlikely because their preservation in this scenario would necessitate significant (>420 km) dextral translation and negligible uplift and erosion, which would remove them from the landscape. This conflicts with known long-term Alpine Fault kinematics (Herman et al., 2009; Tippett & Kamp, 1993). Hence, we inferred a source region to the southwest of the study area, within the Fiordland block. Nonetheless, the basement slivers may be correlated with plutonic suites exposed in either part of the South Island, considering that most of these suites were laterally extensive prior to their dismemberment, uplift, and erosion. We therefore compare our data against that published for each granitic suite within the Tuhua Intrusives, regardless of their present-day geographic location. The petrographic and zircon U-Pb characteristics of these suites are summarized in Table 2.

#### 5.2.1. 121 Ma Diorite and 112 Ma Granodiorite

Considering U-Pb ages and uncertainties, and petrographic variability within each granitoid suite, the 121 Ma hornblende-biotite diorite and the 112 Ma biotite-muscovite granodiorite may be correlated to the Separation Point Suite (± Western Fiordland Orthogneiss (WFO)) or the Rahu Suite (cf. Tables 1 and 2). The data rule out correlation with the other granitoid suites or with the Indecision Creek Complex, which consists predominantly of quartz diorite and was emplaced at c. 124–135 Ma (Allibone, Jongens, Scott, et al., 2009; Bradshaw, 1990). In addition, correlation of the 121 Ma diorite with the Arthur River Complex, which consists of metadiorite to gabbro emplaced at 134 Ma and metamorphosed at 120 Ma (Tulloch et al., 2011), is unlikely given the lack of mesoscopic deformation textures and the absence of metamorphic zircon in the 121 Ma diorite, and additionally because the Arthur River Complex does not physically intersect the Alpine Fault (Turnbull et al., 2010).

To discriminate between possible correlations, we compare zircon trace-element data from our Cretaceous samples to those published for the Separation Point Suite, Rahu Suite, and WFO (Bolhar et al., 2008; Hiess et al., 2015; Schwartz et al., 2017).

U/Yb values in zircon are a proxy for the relative contribution of crustal sources to the parent magma at the time of zircon crystallization (Grimes et al., 2007, 2015; Jara et al., 2021). This is because U is enriched and Yb is slightly depleted in arc magmas and continental crust relative to mid-ocean ridge basalt mantle (Kelemen et al., 2014). Hence, crustal inputs tend to increase parent magma U/Yb. Zircon has nearly equivalent affinities for these elements (Bea et al., 1994), and so it records magma U/Yb values at the time of crystallization. Melt differentiation may also increase U/Yb values due to the partitioning of Yb by many common accessory minerals (including

MERE ET AL. 16 of 34

 Table 2

 Summary Features of Paleozoic-Mesozoic Tuhua Intrusive Granitoid Suites

		Granite		Mineralogy		Magmatic zircon
Suite	Terrane	type	Predominant lithology (outliers)	Mafic	Accessoryb	<sup>206</sup> Pb/ <sup>238</sup> U age (outliers) <sup>c</sup>
Karamea Suite	Buller	S	Granite to bt-rich tonalite	Bt ± Msc	Ttn, Aln, Ilm	368–370 (363–379)
Paringa Suite	Buller, Takaka	I	Granodiorite to diorite (gabbro to ultramafic)	Hbl, Bt	Mag, Ttn, Ep	362–369
Ridge Suite	Takaka (Buller)	S	Granite to granodiorite (tonalite)	Bt	Ttn, Ilm	345-364 (c.340-c.365)
Tobin Suite	Buller, Takaka	I	Granite to diorite trondhjemite	Hbl, Bt	Mag, Ttn	342–351
Foulwind Suite	Buller, Takaka	A	Bt-granite to Bt-Msc granite (Afs-granite, diorite)	Bt, Amp, Px	Mnz, Grt, Ilm, Xtm	305–350
Darran Suite	Takaka	I	Gabbro to granodiorite (tonalite to granite)	Hbl, Bt, ±Cpx	Ttn, Mag, Ilm, ±Aln	126–160 (170–177) (224– 232) <sup>d</sup>
Separation Point Suite (non- WFO <sup>e</sup> )	Buller, Takaka	Ι	Granite to diorite	Bt, ±Hbl (Msc)	Ttn, ±Aln, ±Ep (Grt)	111–122 (126–128)
Separation Point Suite (WFO <sup>e</sup> )	Takaka	-	Diorite to monzodiorite (ultramafic, monzonite)	Hbl, Cpx, Opx, ±Bt, ±Ep, ±Grt	±Ttn, ±Rt, ±Aln	115–129
Rahu Suite	Buller	I/S	Granite to granodiorite (tonalite to diorite)	Bt, $\pm$ Hbl (Msc)	Ttn, Aln, ±Ep, ±Tur	109–115 (126–131)

Note. Mineral abbreviations follow Whitney and Evans (2010): Afs, alkali feldspar; Aln, allanite; Amp, amphibole; Bt, biotite; Cpx, clinopyroxene; Ep, epidote; Grt, garnet; Hbl, hornblende; Ilm, ilmenite; Mag, magnetite; Mnz, monazite; Msc, muscovite; Opx, orthopyroxene; Px, pyroxene; Rt, rutile; Ttn, titanite; Tur, tourmaline; Xtm, xenotime. WFO, Western Fiordland Orthogneiss. Data compiled from Allibone and Tulloch (2004), Allibone et al. (2007), Allibone, Jongens, Scott, et al., 2009, Allibone, Jongens, Turnbull, et al. (2009), Ballard (1989), Bolhar et al. (2008), Cox and Barrell (2007), Decker (2016), Gibson (1982), Gollan (2006), Hiess et al. (2010), Hollis et al. (2003, 2004), Hout et al. (2012), Johnston (1990), Kimbrough et al. (1994), Klepeis et al. (2016), McCoy-West et al. (2014), Muir et al. (1994, 1997, 1998), Nathan et al. (2002), Ramezani and Tulloch (2009), Rattenbury et al. (1998), Ryland (2011), Sagar et al. (2016), Schwartz et al. (2016), Scott and Palin (2008), Scott et al. (2008), Tulloch and Challis (2000), Tulloch and Kimbrough (2003), Tulloch et al. (2009), Tulloch and Kimbrough (1989), Turnbull et al. (2016), Waight et al. (1997), and Ward (1984). \*Excluding the minor Rotoroa Suite (156 ± 2 Ma; Kimbrough et al., 1993). \*Excluding zircon, apatite, ±opaque oxide. \*Reported in Ma. \*Western Fiordland Orthogneiss is a group of granitic-dioritic plutons derived from partial melting of the Separation Point Suite at lower crustal pressure-temperature conditions (Schwartz et al., 2017; references therein). \*dEmplacement involved multiple distinct pulses of magmatism.

zircon itself, Bea, 1996). We therefore evaluated U/Yb values against Hf concentration, which is a monitor of melt differentiation (Claiborne et al., 2006; Grimes et al., 2007), to compare distinct groups of data.

The rare-earth element compositions of zircon are an additional independent proxy of parent magma and/or rock composition at the time of zircon crystallization (Belousova et al., 2002; Heaman et al., 1990; Nardi et al., 2013). In addition, these compositions may also indicate the presence of co-crystallizing phases that have contrasting rare-earth affinities to zircon (Brophy, 2008; Fujimaki, 1986; Grimes et al., 2015; Rubatto & Hermann, 2007; Schwartz et al., 2017). We follow Grimes et al. (2015) by leveraging the concentrations of light and middle rare-earth elements relative to heavy rare-earth elements, as recorded by Ce/Yb and Gd/Yb values, respectively.

The zircon trace-element data support two interpretations: (a) the 121 Ma diorite and the 112 Ma granodiorite crystallized from a chemically similar parent magma, and (b) both of these units are correlatives of the Western McKerr Intrusives (WMI) component of the WFO. These interpretations are supported by comparable trends in both magma enrichment (U/Yb vs. Hf, Figure 6a) and rare-earth element compositions (overlap in Gd/Yb vs. Ce/Yb space, Figure 6b) between our samples, the WMI, and a  $113.4 \pm 1.0$  Ma biotite-muscovite granite dike that intrudes the WMI near Caswell Sound (Schwartz et al., 2017). Moreover, interpretation (ii) is consistent with existing zircon U-Pb data. Of the constituent plutons within the WFO, the emplacement age of the 121 Ma hornblende-biotite diorite is most similar to zircon crystallization ages in the WMI (Schwartz et al., 2017). Likewise, petrographic and zircon U-Pb similarities between the 112 Ma biotite-muscovite granodiorite and the 113 Ma biotite-muscovite granite dike in the WMI further support a correlation. We therefore infer that a 112–113 Ma pulse of WMI related magmatism may have resulted in the emplacement of a comparatively more fractionated granite, likely involving light and middle rare-earth fractionation by monazite, apatite, and titanite (Table 1, Figure 6b, Grimes et al., 2015).

MERE ET AL. 17 of 34

5252027, 2024, 11, Downloaded from https://agupubs

online library wiley com/doi/10.1029/2024GC011839, Wiley Online Library on [12/03/2025]. See the Terms and Conditions

#### 5.2.2. 351 Ma Monzogranite and Monzogranite Gneiss

We infer that the biotite monzogranite and monzogranite gneiss are correlated with Ridge Suite S-type granitoids that outcrop in both the Fiordland and Nelson blocks. The 351 Ma emplacement age of the monzogranitic units is notably similar to the emplacement ages of the Ridge Suite, the Tobin Suite, and the Foulwind Suite (Tables 1 and 2). However, petrographic and zircon U-Pb characteristics are most consistent with an S-type character, and hence, correlation to the Ridge Suite. First, mineral assemblages of the monzogranitic units match those of S-type granites; this includes an absence of amphibole and pyroxene, the presence of monazite as a primary mineral, comparable proportions of microcline to plagioclase, and lack of pink alkali feldspar (Chappell & White, 1974, 2001; Whalen et al., 1987). Second, an abundance of inherited zircon present as core domains is consistent with models of inherited zircon survival during petrogenesis of peraluminous S-type granites (Bea et al., 2021). Third, inherited zircons have modes that are similar to inherited zircons in both the Ridge Suite and Karamea Suite (c. 500–600 Ma and c. 900–1,100 Ma, Muir et al., 1996; Tulloch et al., 2009), and additionally to prominent age modes of Takaka Terrane detrital zircon populations (Adams et al., 2015; Irel & Gibson, 1998; Ireland, 1992).

The biotite-tonalite All Round Pluton, which intrudes Takaka Terrane country rock in Secretary Island, is the nearest Ridge Suite pluton to the Alpine Fault in Fiordland. The mineralogy, texture, and  $347.75 \pm 0.86$  Ma emplacement age of this pluton (Allibone, Jongens, Turnbull, et al., 2009; Ramezani & Tulloch, 2009) are all similar to those of the 351 Ma biotite monzogranite. Other Ridge Suite plutons with similar characteristics (351–354 Ma, biotite granite-granodiorite; Allibone, Jongens, Turnbull, et al., 2009; Tulloch et al., 2009) outcrop in southwestern Fiordland.

#### 6. Discussion

#### 6.1. Fault-Sliver Source Area

Correlation of the fault-bounded slivers of crystalline basement to the WMI and the Ridge Suite allows us to infer the source region in coastal or offshore Fiordland from which they were displaced. For this purpose, basement lithologies that are correlated with the WMI are particularly diagnostic. This is because the WMI crop out for just 18 km along the length of the Fiordland coastline, approximately between Caswell Sound and a small unnamed stream north of Looking Glass Bay (see WMI in Figure 7). Aside from this study, correlated rocks have not been mapped elsewhere in New Zealand.

Conversely, the data do not likely constrain the source location of the Ridge Suite-correlated monzogranite. As previously mentioned, the petrographically and geochronologically similar All Round Pluton crops out near the offshore part of the Alpine Fault on Secretary Island (Figure 7). We view correlation to this specific pluton as unlikely because lateral separation of ~24 km between it and the WMI implies a similar amount of dextral displacement between the slivers, yet field mapping shows an intrusive relationship, and hence, a close spatial association between these two lithologies prior to their dismemberment. Zircon U-Pb data also support this association because the metamorphic age of the Ridge Suite-correlated monzogranite gneiss closely matches the emplacement age of the WFO near Caswell Sound (WMI and Misty Pluton, Klepeis et al., 2004; Schwartz et al., 2017). If the Ridge Suite-correlated monzogranite is indeed correlated to the All Round Pluton, we infer that it is derived from somewhere in coastal Fiordland other than near Secretary Island.

Our analysis shows that basement rocks from the Pacific Plate have been fragmented by the Alpine Fault Zone, have been displaced by strike-slip motion, and are now captured by the Australian Plate. The basement units we correlate to the WMI can thus be used to constrain a component of the Alpine Fault offset. To this end, we linearly projected the northeastern and southwestern contacts of the WMI at the Fiordland coastline toward the northwest and into the bathymetric trace of the offshore southern Alpine Fault. We perform a similar linear projection of the displaced fragments in the Kaipo Valley to the southeast into the active strand of the Alpine Fault. These linear approximations are undoubtedly simplifications; however, there is currently no data to constrain an alternative geometry of the WMI offshore of Fiordland, and our mapping suggests that the displaced correlatives are limited to a small  $\sim$ 2 km-long sliver in the Kaipo Valley. We therefore view our choice of projection as a minimally interpretive one that allows for the displaced units and their source outcrop to be used as approximated offset markers. Measured along the fault trace, the minimum and maximum distances between where these projections intersect the fault constrain  $\sim$ 70–90 km of cumulative dextral displacement on the presently active strand of the southern Alpine Fault (Figure 7). Alternative pre-displacement geometries and/or a component of vertical

MERE ET AL. 18 of 34

15252027, 2024, 11, Downloaded from https://agupubs.onlinelibrary.wiley.com/doi/10.1029/2024GC011839, Wiley Online Library on [12/03/2025]. See the Terms and Conditions (https://onlinelibrary.wiley.com/term

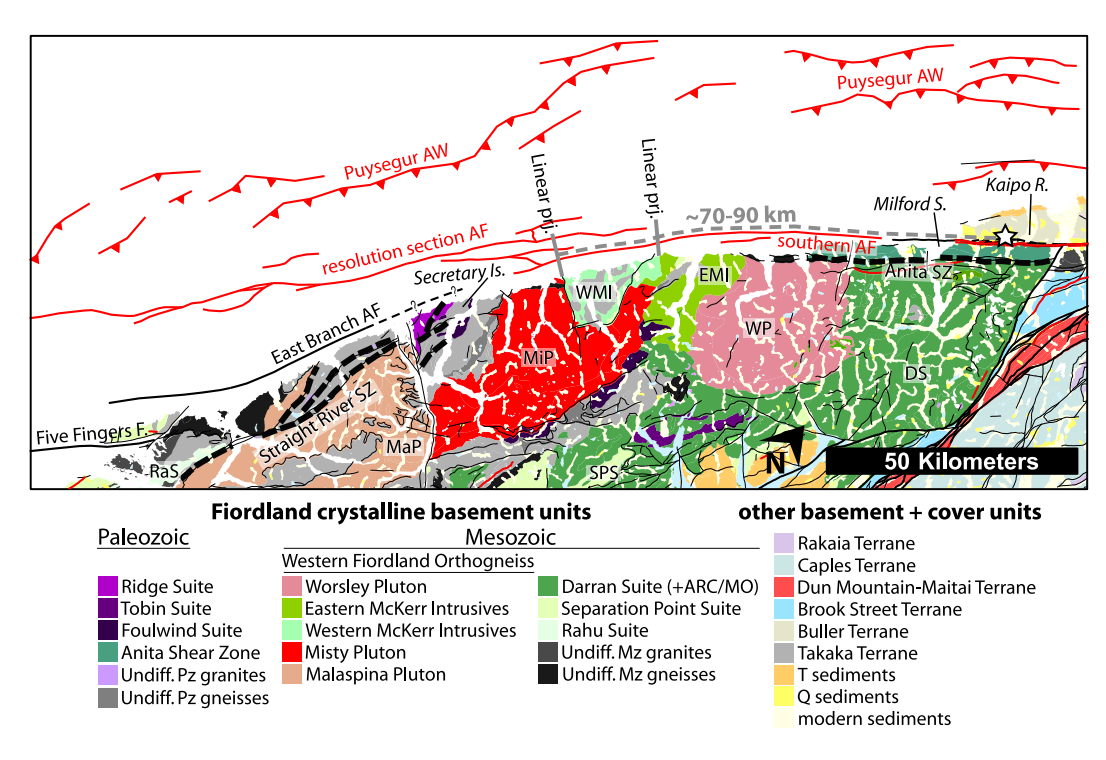


**Figure 7.** Geological map of western Fiordland. White star depicts present-day location of displaced correlatives of the Western McKerr Intrusives (WMI) and Ridge Suite in the field area. Gray lines show offshore linear extrapolation of WMI contacts; dashed line shows displacement by the southern Alpine Fault. Basement geology was modified from Turnbull et al. (2010). Offshore faults are derived from Lebrun et al. (2000) and Barnes et al. (2002, 2005).

displacement could contribute to uncertainty in this measurement, although these factors are not quantifiable with presently available data. Material transfer between the Pacific-Australian Plates is uncommon on the Alpine fault; to our knowledge, all previous examples involve abandonment by reverse faulting (Ghisetti, 2022; Norris & Cooper, 1995, 1997; Rattenbury et al., 2010; Toy et al., 2011).

#### 6.2. Slip History of the Southern Alpine Fault

The  $\sim$ 70–90 km of dextral displacement we estimate on the presently active strand of the southern Alpine Fault is much lower than the 460–480 km of post-Oligocene displacement on the central and northern sections of the fault (Hunt, 1978; Mortimer, 2014; Sutherland et al., 2000; Wellman, 1956). This seems to imply a steep south-decreasing gradient in cumulative displacement. One hypothesis for this discrepancy may be that some post-Oligocene displacement has been transferred away from the southern Alpine Fault and onto other faults in southwest New Zealand. Another hypothesis that does not necessarily require any gradient in cumulative displacement is that the basement slivers record incremental, rather than cumulative, Alpine Fault displacement.

Regarding the first hypothesis, some tectonic reconstructions have inferred that large magnitudes of northeast-southwest oriented fault displacement have occurred south of the Alpine Fault during the Miocene-Pliocene (Furlong & Kamp, 2009; Ghisetti, 2022; P. R. King, 2000; LeBrun et al., 2003; Stock & Molnar, 1982; Walcott, 1989). Many independent studies support the southward transfer of some slip away from the southern Alpine Fault, primarily by dextral and/or reverse displacement on the Moonlight-Hauroko Fault System, Hollyford Fault System, Livingstone Fault, Glade-Darran Fault, and offshore Taurau Fault (Figure 1b; Beggs & Ghisetti, 2006; Blattner, 1991; Constantine, 1987; Lamb et al., 2016; Shuck et al., 2021; Sutherland & Melhuish, 2000; Sutherland et al., 2009; Turnbull & Uruski, 1995; Turnbull et al., 1975; Uruski, 1992), on faults within Fiordland (Klepeis, Webb, Blatchford, Jongens, et al., 2019; Klepeis, Webb, Blatchford, Schwartz, et al., 2019), and eastwest shortening in basins in southwest Zealandia (Beggs & Ghisetti, 2006; Melhuish et al., 1999; Norris & Carter, 1980; Norris & Turnbull, 1993; Sutherland et al., 2006).

MERE ET AL. 19 of 34

15252027, 2024, 11, Downloaded from https://agupubs.onlinelibrary.wiley.com/doi/10.1029/2024GC011839, Wiley Online Library on [12/03/2025]. See the Terms and Conditional Cond

Regarding the second hypothesis, existing geological estimates show roughly constant strike-slip rates on the southern parts of the Alpine Fault since the late Pleistocene. This includes strike-slip rates estimates of 29.6 (-2.5/+4.5) mm a<sup>-1</sup> since c. 270 ka averaged along the onshore southern section (Barth et al., 2014) and 27.2 (-3.0/+1.8) mm a<sup>-1</sup> to 31.4 (-3.5/+2.1) mm a<sup>-1</sup> since c. 17 ka along the offshore southern and Resolution sections (Barnes, 2009). In addition, Sutherland (1994) used provenance analysis of an offset Fiordland-sourced conglomerate to estimate a strike-slip rate of 27–35 mm a<sup>-1</sup> since c. 3.6 Ma averaged across the southern onshore and offshore parts of the plate boundary. Although this estimate is not strictly an Alpine Fault strike-slip rate, it nonetheless suggests that at least ~95 km of right-lateral displacement has been accommodated between coastal Fiordland and present-day South Westland since the late Pliocene. Farther north, along the central Alpine Fault, Norris and Cooper (2003) use strain estimates derived from exhumed mylonites to estimate ~55–170 km of oblique-dextral shear within the ductile roots of the fault system, which they inferred has accumulated since c. 5 Ma. Despite considerable uncertainty in this estimate, it supports similar amounts of Plio-Quaternary displacement on the central and southern sections.

Considering both the timing of deformation in southwest Zealandia and the apparent temporal uniformity of strike-slip rates on the Alpine Fault and averaged across the plate boundary since the middle Pliocene, we infer that the displaced basement slivers record an incremental displacement. In this case,  $\sim$ 70–90 km of displacement implies capture of Fiordland basement rocks by the Australian plate by c. 2.0–3.3 Ma. It should be noted that the approximate age of this displacement represents a minimum; non-rigid block deformation, partitioned slip within a distributed fault network, and/or the transfer of some Pliocene plate boundary deformation away from the Alpine Fault would all increase the amount of time since the basement slivers have been displaced.

#### 6.3. Tectonic Evolution of the Southern Alpine Fault

We reveal at least four key characteristics of the southernmost ~30 km of the onshore Alpine fault (Figure 4) that provide context to its Plio-Quaternary tectonic evolution. First, the fault zone tapers in plan-view width toward both the northeast and southwest to form a geometry that is reminiscent of an elongated and fault-bisected lozenge. Second, a network of subsidiary faults bifurcates from the principal strand of the Alpine Fault and extends down the central axis of the fault zone. Third, left-stepping (restraining) geometries are common within the fault zone. Fourth, basement units displaced from coastal Fiordland are present within the fault zone and are now captured by the Australian Plate.

Both the geometry of the fault zone and the kinematics associated with the transfer of material from the Pacific Plate to the Australian Plate are consistent with the development and evolution of a restraining stepover in the offshore Alpine Fault (Figure 8). Similar rhomboidal to lozenge-shaped fault zone geometries composed of sigmoidal boundary and interior faults have been mapped at restraining stepovers (and comparatively more evolved bends) in other strike-slip systems (e.g., Barka & Kadinsky-Cade, 1988; Barnes et al., 2005; Dooley & McClay, 1996; Fedorik et al., 2022; Mann & Gordon, 1996; Smith et al., 2007). Mechanical analog experiments of strike-slip restraining stepovers have also reproduced these geometries (Cooke et al., 2013; Dooley et al., 1999; Hatem et al., 2015; McClay & Bonora, 2001; Mitra & Paul, 2011; Richard et al., 1995). Restraining stepovers generally evolve by an early stage of offset master fault linkage by newly formed oblique-motion faults, an intermediate stage of internal deformation within the stepover region, and a late stage involving linkage of the principal displacement zone by mechanically well-oriented strike-slip faults that either dissect or bypass the restraining region (Figure 8; Cooke et al., 2013; McClay & Bonora, 2001; Mitra & Paul, 2011; Scholz et al., 2010). Dissection or bypassing of the restraining geometry means that material formerly located within or near the stepover may become transferred across, and subsequently be displaced by the new principal displacement zone. We infer that the present-day fault zone width of ~1.2 km suggests this was initially a modestly sized stepover along the offshore southern Alpine Fault and not a major structural complexity. Late Quaternary plate boundary deformation has subsequently reactivated and inverted many of the faults within the proposed stepover as normal or dextral-normal structures (Figures 2d and 3d).

Although stepovers and bends are commonly youthful features of immature faults (Mann, 2007; Wesnousky, 1988, references therein), these structural complexities can also develop and/or persist along mature fault systems (e.g., Barnes et al., 2001, 2005; Hatem et al., 2017). One hypothesis we consider is that a restraining stepover formed during the Pliocene in response to a sidewall-ripout of the offshore Alpine Fault. Sidewall-ripouts form along strike-slip faults in cases where frictional adhesion on the principal displacement zone

MERE ET AL. 20 of 34

15252027, 2024, 11, Downloaded from https://agupubs.onlinelibrary.viley.com/doi/10.1029/2024GC011839, Wiley Online Library on [12/03/2025]. See the Terms and Conditions (https://onlinelibrary.viley.com/terms-and-conditions) on Wiley Online Library for rules of use; OA articles are governed by the applicable Creative Commons Licensia

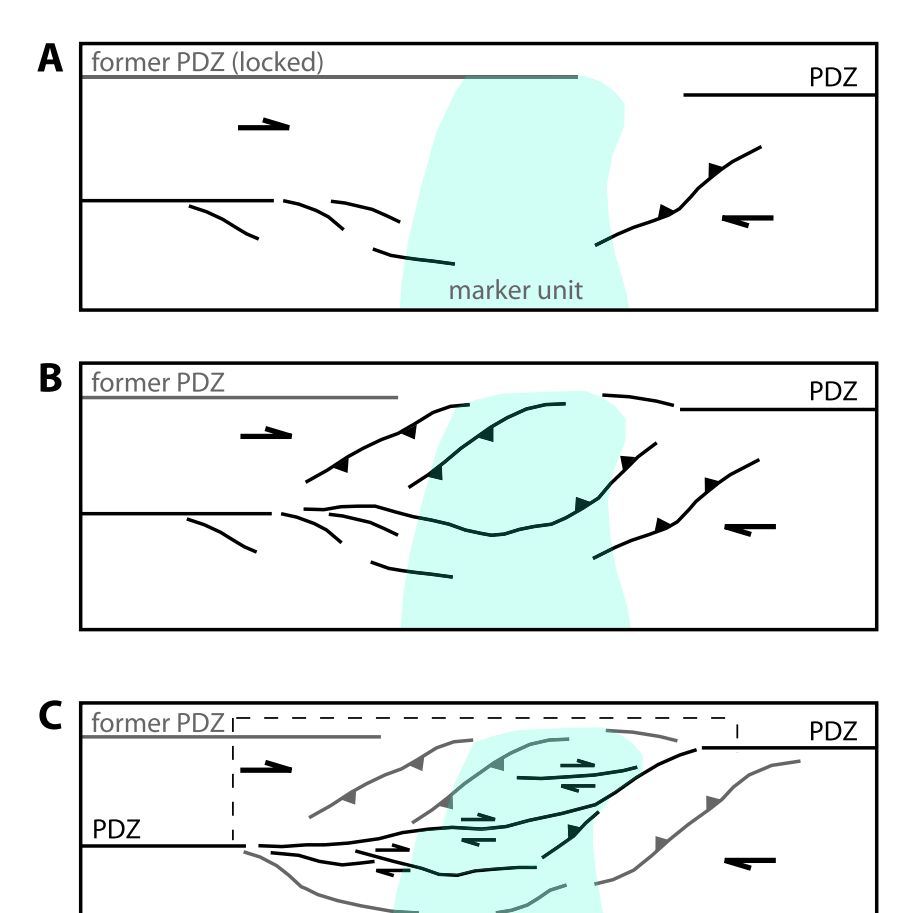


**Figure 8.** Line diagram showing the structural evolution of a strike-slip restraining stepover in a mechanical analog experiment. Black lines depict active faults, gray lines depict inactive faults, and cyan polygon depicts a marker unit that is analogous to the basement units displaced from coastal Fiordland. (a) Early stage. (b) Intermediate stage. (c) Late stage. Note (i) capture of the marker unit dissected by the opposite side of the fault, and (ii) similarity between the fault zone geometry in the dashed region and that shown in Figure 4a. PDZ-principal displacement zone. Modified from McClay and Bonora (2001).

causes slip on a newly formed or reactivated offset fault segment to be mechanically favorable during earthquake ruptures (Figure 8; Swanson, 1989, 2005). These offset fault segments may become linked with the master fault and thereby form part of the new principal displacement zone. A sidewall-ripout involving a left-offset (restraining) fault segment accounts for both the observed fault zone geometry and the transfer of basement material from southeast to northwest, "across" the Alpine Fault.

Pre-existing structures in western Fiordland may have promoted the formation of a sidewall-ripout or otherwise introduced structural complexity by linkage with the Alpine Fault during the Pliocene. Previous work shows that pre-existing structures influence the present-day geometry of the plate boundary at a variety of spatial scales (Barnes et al., 2005; Lebrun et al., 2000; Mortimer, 2018; Shuck et al., 2021; Sutherland & Melhuish, 2000); however, the influence of pre-existing structures on former geometries is less certain. During and before the middle Pliocene, offshore strike-slip motion had not yet fully localized along the Resolution section of the Alpine Fault, and it instead occurred closer to the southwestern Fiordland coastline on the Alpine Fault East Branch and other minor fault systems including the Chalky Fault Zone, the Anchor Fault Zone, and the Five Fingers Fault (Figure 9; Barnes et al., 2005; Lebrun et al., 2000). Together, this system of formerly active faults formed an array that was subparallel to, and ~5–15 km northwest of, the steeply dipping Cretaceous-aged Straight River Shear Zone in western Fiordland (D. S. King et al., 2008). Farther north, in northern Fiordland, the southern Alpine Fault has localized along the western margin of the Anita Shear Zone (Figure 7). Structural and thermochronological

MERE ET AL. 21 of 34

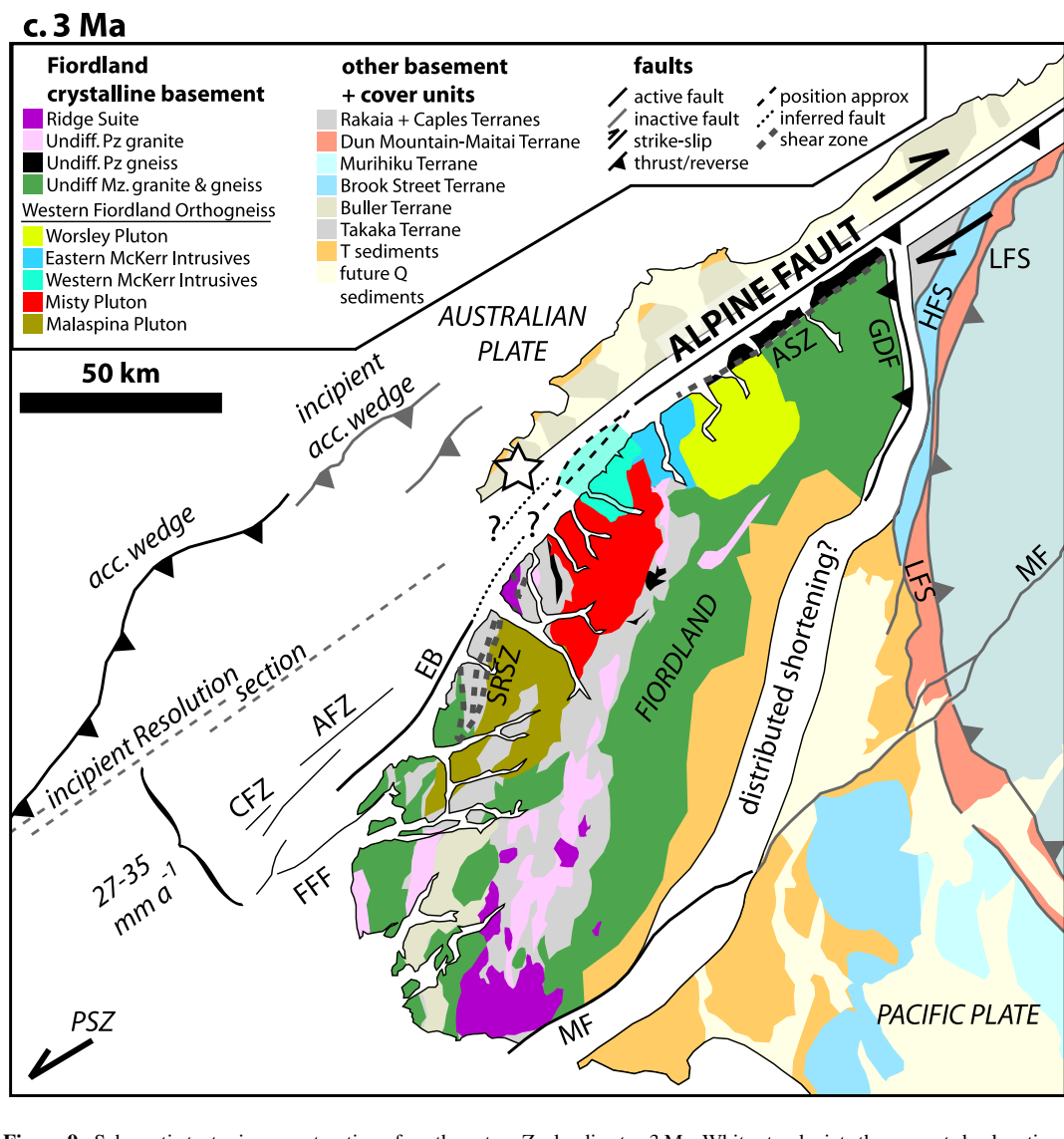


**Figure 9.** Schematic tectonic reconstruction of southwestern Zealandia at c. 3 Ma. White star depicts the present-day location of displaced correlatives of the Western McKerr Intrusives and Ridge Suite. Offshore faults shown as thin lines are presumed to accommodate a subordinate amount of slip relative to the Alpine Fault East Branch. The dextral displacement rate integrated across the entire plate boundary system is from Sutherland (1994). The plate configuration and position of tectonic blocks are derived from the GPlates model of Müller et al. (2019). Basement geology is simplified from Turnbull (2000), Turnbull et al. (2003, 2010), and Rattenbury et al. (2010). Offshore faults are from Lebrun et al. (2000), and Barnes et al. (2005). AFZ, Anchor Fault Zone; ASZ, Anita Shear Zone; CFZ, Chalky Fault Zone; EB, East Branch; FFF, Five Fingers Fault; GDF, Glade Darran Fault; HFS, Hollyford Fault System; MF, Moonlight Fault; LF, Livingstone Fault; acc., accretionary.

data from both shear zones show that they have been reactivated in the late Tertiary by dextral faulting associated with the Australian-Pacific Plate boundary (D. S. King et al., 2008; Klepeis et al., 1999; Klepeis, Webb, Blatchford, Jongens, et al., 2019; Klepeis, Webb, Blatchford, Schwartz, et al., 2019). The offshore intersection of the Alpine Fault East Branch, the Straight River Shear Zone, and the Anita Shear Zone corresponds to the approximate region from where the previously discussed basement fragments have been displaced (Figures 7 and 9).

Collectively, these observations suggest that the locus of strike-slip deformation within the Pliocene offshore plate boundary system was controlled, at least in part, by pre-existing structures in the continental crust of western Fiordland. We hypothesize that prior to the dominance of the Resolution section of the Alpine Fault, the offshore plate boundary system featured a distributed network of active faults that was similar to the branch zones observed

MERE ET AL. 22 of 34

15252027, 2024, 11, Downloaded from https

://agupubs.onlinelibrary.wiley.com/doi/10.1029/2024GC011839, Wiley Online Library on [12/03/2025]. See the Terms and Conditi

near the tips of other strike-slip faults worldwide (Figure 9; Kim & Sanderson, 2006). Recent work shows that in such distributed strike-slip systems, the slip rates of the component faults may vary through time such that they switch back and forth as the most dominant structure while the system-wide (cumulative) displacement rate remains constant (Dolan et al., 2024). This effect means that the principal displacement zone may be a transient feature; the presence of pre-existing structures in western Fiordland may have facilitated such behavior. One implication of our model of the Pliocene offshore plate boundary system is the presence of an inactive "former" principal displacement zone segment along the offshore southern Alpine Fault, perhaps near Milford Sound (Figures 7 and 8). There are no presently available data to evaluate this prediction. However, southwest of here, inactive faults have been imaged using seismic reflection to the northwest of the southern Alpine Fault; these may be analogous features (Barnes et al., 2005).

Since the Pliocene, northeastward translation of the Australian Plate has progressively juxtaposed the western margin of a failed Eocene-Oligocene aged rift against the plate boundary, resulting in the development of the Resolution section (Barnes et al., 2005; Lebrun et al., 2000, 2003; Shuck et al., 2021). Under thrusting of the Australian Plate in the Puysegur accretionary wedge propagated northeastwards during this time (Barnes et al., 2002). This leads us to infer that the Resolution section may have developed along a similar trajectory to eventually link with the southern Alpine fault. The transfer of dextral slip onto the comparatively more localized Resolution section likely drove the abandonment of the distributed plate boundary system that was farther to the east (Figure 9).

#### 6.4. Modern Seismotectonic Implications

A  $\sim$ 4 kyr paleoseismic record shows temporal switching between multi-section ( $M_w \sim 8$ ) and single-section ( $M_w \sim 7$ ) Alpine Fault earthquakes, and in addition, that about one-half of ruptures have terminated at or near the central-southern section boundary (Howarth et al., 2018, 2021). Using multi-cycle earthquake simulations, Howarth et al. (2021) suggested that fault geometry is a primary control on this observed earthquake behavior; their model projected surficial fault dips to depth and incorporated a continuous corkscrew-like twist in the fault plane near the central-southern section boundary. The crustal-scale structure of the southern Alpine Fault is nonetheless debated, and alternative models exist, including a low-angle crustal detachment that extends southwestward from the central to the southern section (Lamb et al., 2015; Warren-Smith et al., 2016) or structural segmentation between a moderately dipping, listric central segment and subvertical southern segment (Koons et al., 2003; Warren-Smith et al., 2022). Statistical analysis of historic rupture extents on other major strike-slip faults (Biasi & Wesnousky, 2016, 2017, 2021; Wesnousky, 1988, 2006) and dynamic simulations of earthquakes (Duan & Oglesby, 2005; Harris & Day, 1999; Lozos, 2021; Lozos et al., 2011) both independently support the concept that certain fault configurations can arrest earthquake ruptures, although this effect is geometry-dependent.

Our mapping helps to refine the major structural geometry of the southern Alpine Fault. In the absence of rigorous geophysical imaging (e.g., Davey et al., 2007; Stern et al., 2007), this data may aid the parameterization of future earthquake modeling studies. We hypothesize that much of the fine-scale complexity ( $10^{-1}$  km-scale) in geomorphic fault expression corresponds to shallow distributed faulting. Previous studies show that fault zones are typically more localized in bedrock than in sedimentary deposits (Oskin et al., 2012; Reid, 1910; Rodriguez Padilla et al., 2022; Tchalenko & Ambraseys, 1970; Tchalenko & Berberian, 1975). This effect increases with the ratio of overburden thickness to cumulative fault displacement in the overburden (Bray et al., 1994; Naylor et al., 1986; Quigley et al., 2012; Richard et al., 1995; Tchalenko, 1970). We show that the width of the subsidiary fault zone, variance in the subsidiary fault strike, and variance in the subsidiary fault scarp aspect are all locally elevated where the fault is covered by late Quaternary glacial deposits (Figures 2 and 3). This relation suggests that much of the subsidiary faulting associated with the Alpine Fault is restricted to the overburden. We infer that localized geomorphic fault expression in some other areas of thick sedimentary cover (e.g., coastal plains and major valleys, Figures 1b and 2) results from recently active surface processes that have obscured evidence of distributed subsidiary faulting (Lukács et al., 2019) and/or from coseismic liquefaction of water-saturated sediments, which inhibits shear deformation from localizing onto discrete structures (Fletcher et al., 2014; Oskin et al., 2012).

Conversely, we infer that the major geomorphic features of the southern Alpine Fault ( $10^0$  km-scale) reflect fault zone structure that extends deeper into the brittle crust. Our geologic mapping along the southernmost onshore

MERE ET AL. 23 of 34

somewhat misaligned along-strike.

Alpine Fault supports this interpretation in that we reveal the partial reactivation of fault arrays that likely extend to several kilometers of crustal depth (Figure 4b). The most prominent geomorphic and/or structural features of the southern Alpine fault are the extensional stepover and restraining bend in the primary trace that occur alongstrike of each other ~5–15 km southwest of central-southern section boundary in the Cascade River valley (Figures 2b and 3). Berryman et al. (1992) previously interpreted the former of these as a strike-slip duplex composed of two laterally continuous fault planes that merge at an unspecified depth in the upper crust. Our mapping shows the apparent segmentation of primary fault traces; there are no laterally continuous rupture pathways, even where fault offsets are formed directly in bedrock (west of the Cascade River, Figure 2b). In addition, fault scarps associated with these primary fault traces are everywhere southeast-facing (Figure 3d) rather than facing toward the center of the stepover, the latter of which is common in rooted strike-slip pull-apart structures (Dooley, 1994; Rahe et al., 1998). In our view, these characteristics may be consistent with segmentation between two discrete structures, rather than indicative of shallow distributed faulting above a single continuous non-planar fault at depth. The spatial correlation of an extensional stepover and a restraining bend in the Alpine Fault is also conspicuous within the framework of a continuous non-planar fault; if this region instead represents a segment boundary, this spatial correlation may suggest that the two interacting segments are

Considering that our data cannot definitively rule out the possibility of a single continuous structure at depth, however, an alternative hypothesis may be that structural complexities along the southern Alpine Fault reflect lateral variation in the crustal depth from which the fault has been exhumed (Tippett & Kamp, 1993). Although this hypothesis may explain the preservation of inactive structural complexity along the southern Alpine Fault near the Kaipo valley, we do not favor it because abrupt lateral changes in fault zone structure, kinematics, and seismicity between the central and southern sections imply a similarly steep gradient in the magnitude of exhumation. If fault segments within the step do indeed merge at depth, locally steep near-surface fault dips (~70–80°; Barth et al., 2013) and an assumption of roughly planar faults imply this occurs at ~4–5 km.

Existing statistical analysis of earthquakes worldwide suggests that geometric complexity near the central-southern section boundary has about a 30%–40% probability of arresting earthquake rupture, subject to the interpretation of fault structure from geomorphic expression (Biasi & Wesnousky, 2021). However, in some recent earthquakes around the world, ruptures have spanned much larger geometric complexities and/or have linked multiple structures or segments together in joint ruptures (e.g., Biasi & Wesnousky, 2016, 2017; Fletcher et al., 2014; Litchfield et al., 2018; Sieh et al., 1993). These events underscore the usefulness of physics-based earthquake simulations in delineating possible future rupture scenarios. Our analysis suggests that future simulations of Alpine Fault earthquakes may reasonably consider testing both a segmented fault geometry and the continuous twist-at-depth model presently implemented in the New Zealand Community Fault Model version 1.0 (Seebeck et al., 2024). Our new constraints on shallow fault zone structure and late Cenozoic tectonic evolution highlight the need for improved constraints on the deeper crustal structure of the Alpine Fault, particularly near and along the central-southern section boundary.

#### 7. Conclusions

We present a multidisciplinary analysis of the southern Alpine Fault and characterize its Plio-Quaternary slip history, tectonic evolution, and fault zone structure. New constraints on these characteristics are derived from the integration of geologic-geomorphic mapping and the identification and correlation of fault-offset basement units.

Our analysis shows that crystalline basement units derived from coastal Fiordland have been fragmented by the southern Alpine Fault Zone and captured by the Australian Plate. The apparent dextral offset of these units implies a displacement of ~70–90 km on the presently active strand of the southern Alpine Fault that we infer is of Plio-Quaternary age. Interpretation of fault zone structure and kinematics suggests that these units have been displaced following the development and dissection or bypassing of a minor strike-slip restraining stepover along the offshore southern Alpine Fault. This minor stepover may reflect a sidewall-ripout. We reconstruct the plate boundary at c. 3 Ma and show that during this time, the offshore plate boundary likely featured a distributed network of active faults that exploited pre-existing structures in the continental crust of the Pacific Plate. The subsequent localization of strike-slip deformation farther west has driven the abandonment of this system. Our analysis contributes to a view of the southern Alpine Fault as a structure that has evolved within a dynamic plate boundary system, and that may be less structurally mature than other parts of the fault to the northeast.

MERE ET AL. 24 of 34

15252027, 2024, 11, Downloaded from https://agupubs.onlinelibrary.wiley.com/doi/10.1029/2024GC011839, Wiley Online Library on [12/03/2025]. See the Terms and Conditions (https://onlinelibrary.wiley.com/terms/

-and-conditions) on Wiley Online Library for rules of use; OA articles are governed by the applicable Creative Commons Licens

25 of 34

Acknowledgments

awarded to N.C. Barth.

MERE ET AL.

We thank Virginia Toy and Tim Little for

strengthened this manuscript. Appreciation to Whitney Behr for editorial handling.

This research was supported by University

of California Riverside start-up funds

detailed peer-reviews that greatly

Onshore, detailed mapping reveals differences in the geomorphic expression of the southern and central Alpine Faults. Although much of the fine-scale complexity developed in geomorphic fault zone expression reflects shallow distributed faulting, we infer that larger-scale features reflect the penetrative structure of the southern Alpine Fault. We emphasize the importance of geomorphic and/or structural complexity that is immediately southwest of the central-southern section boundary. Here, we hypothesize that a prominent releasing stepover in the fault plane likely penetrates to a seismogenic depth. In our view, the lack of geomorphic evidence for a thoroughgoing rupture pathway across this stepover and its spatial correlation of it with a restraining bend in the Alpine Fault may be consistent with segmentation between two distinct and somewhat misaligned structures. Considering that this region of structural complexity corresponds to the location of several Holocene earthquake rupture terminations (Howarth et al., 2021), and that there is presently little direct geophysical constraint on deeper fault geometry, we suggest that a segmented geometry appears as viable as the continuous fault plane geometry presently implemented in the New Zealand Community Fault Model. Our work underscores the need for future studies of the crustal geometry of the southern Alpine Fault.

#### **Conflict of Interest**

The authors declare no conflicts of interest relevant to this study.

# **Data Availability Statement**

Complete field and petrographic descriptions of map units shown in Figure 4, field locations visited in-person, and zircon isotopic data are provided in Supporting Information S1. Detailed active fault trace maps are provided as ESRI shapefiles in Mere and Barth (2024). We used the freely available Isoplot 4.0 software (Ludwig, 2009) for common-lead correction, age calculations, and visualization of LASS-ICP-MS U-Pb isotopic data.

#### References

Adams, C. J., Mortimer, N., Campbell, H. J., & Griffin, W. L. (2015). Detrital zircon ages in Buller and Takaka terranes, New Zealand: Constraints on early Zealandia history. New Zealand Journal of Geology and Geophysics, 58(2), 176–201. https://doi.org/10.1080/00288306.2015.

Allibone, A. H., Jongens, R., Scott, J. M., Tulloch, A. J., Turnbull, I. M., Cooper, A. F., et al. (2009). Plutonic rocks of the Median Batholith in eastern and central Fiordland, New Zealand: Field relations, geochemistry, correlation, and nomenclature. New Zealand Journal of Geology and Geophysics, 52(2), 101–148. https://doi.org/10.1080/00288300909509882

Allibone, A. H., Jongens, R., Turnbull, I. M., Milan, L. A., Daczko, N. R., DePaoli, M. C., & Tulloch, A. J. (2009). Plutonic rocks of Western Fiordland, New Zealand: Field relations, geochemistry, correlation, and nomenclature. *New Zealand Journal of Geology and Geophysics*, 52(4), 379–415. https://doi.org/10.1080/00288306.2009.9518465

Allibone, A. H., & Tulloch, A. J. (2004). Geology of the plutonic basement rocks of Stewart Island, New Zealand. New Zealand Journal of Geology and Geophysics, 47(2), 233–256. https://doi.org/10.1080/00288306.2004.9515051

Allibone, A. H., Turnbull, I. M., Tulloch, A. J., & Cooper, A. F. (2007). Plutonic rocks of the Median Batholith in southwest Fiordland, New Zealand: Field relations, geochemistry, and correlation. New Zealand Journal of Geology and Geophysics, 50(4), 283–314. https://doi.org/10.1080/00288300709509838

Almond, P. C., & Tonkin, P. J. (1999). Pedogenesis by upbuilding in an extreme leaching and weathering environment, and slow loess accretion, south Westland, New Zealand. *Geoderma*, 92(1–2), 1–36. https://doi.org/10.1016/s0016-7061(99)00016-6

Ando, R., Imanishi, K., Panayotopoulos, Y., & Kobayashi, T. (2017). Dynamic rupture propagation on geometrically complex fault with along-strike variation of fault maturity: Insights from the 2014 Northern Nagano earthquake. Earth, Planets and Space, 69, 1–13. https://doi.org/10.1186/s40623-017-0715-2

Antoine, S. L., Klinger, Y., Delorme, A., & Gold, R. D. (2022). Off-fault deformation in regions of complex fault geometries: The 2013, Mw7. 7, Baluchistan Rupture (Pakistan). *Journal of Geophysical Research: Solid Earth*, 127(11), e2022JB024480. https://doi.org/10.1029/2022jb024480

Arden, J. W. (1977). Isotopic composition of uranium in chondritic meteorites. *Nature*, 269(5631), 788–789. https://doi.org/10.1038/269788a0
Atwater, T. (1970). Implications of plate tectonics for the Cenozoic tectonic evolution of western North America. *Geological Society of America Bulletin*, 81(12), 3513–3536. https://doi.org/10.1130/0016-7606(1970)81[3513:ioptft]2.0.co;2

Ballard, H. R. (1989). Permian arc volcanism and aspects of the general geology of the Skippers Range, NW Otago (Doctoral Dissertation). University of Otago.

Barka, A. A., & Kadinsky-Cade, K. (1988). Strike-slip fault geometry in Turkey and its influence on earthquake activity. *Tectonics*, 7(3), 663–684. https://doi.org/10.1029/tc007i003p00663

Barnes, P. M. (2009). Postglacial (after 20 ka) dextral slip rate of the offshore Alpine fault, New Zealand. *Geology*, 37(1), 3–6. https://doi.org/10.1130/g24764a.1

Barnes, P. M., Bostock, H. C., Neil, H. L., Strachan, L. J., & Gosling, M. (2013). A 2300-year Paleoearthquake record of the southern Alpine Fault and Fiordland Subduction zone, New Zealand, based on stacked Turbidites. *Bulletin of the Seismological Society of America*, 103(4), 2424–2446. https://doi.org/10.1785/0120120314

Barnes, P. M., Davy, B., Sutherland, R., & Delteil, J. (2002). Frontal accretion and thrust wedge evolution under very oblique plate convergence: Fiordland Basin, New Zealand. *Basin Research*, 14(4), 439–466. https://doi.org/10.1046/j.1365-2117.2002.00178.x

15252027, 2024, 11, Downloaded from https

onlinelibrary.wiley.com/doi/10.1029/2024GC011839, Wiley Online Library on [12/03/2025]. See the Terms

the applicable Creative Commons License

- Barnes, P. M., Sutherland, R., Davy, B., & Delteil, J. (2001). Rapid creation and destruction of sedimentary basins on mature strike-slip faults: An example from the offshore Alpine Fault, New Zealand. *Journal of Structural Geology*, 23(11), 1727–1739. https://doi.org/10.1016/s0191-8141 (01)00044-x
- Barnes, P. M., Sutherland, R., & Delteil, J. (2005). Strike-slip structure and sedimentary basins of the southern Alpine Fault, Fiordland, New Zealand. *Geological Society of America Bulletin*, 117(3–4), 411–435. https://doi.org/10.1130/b25458.1
- Barrell, D. J. A. (2011). Quaternary glaciers of New Zealand. In Developments in quaternary sciences (Vol. 15, pp. 1047–1064). Elsevier. https://doi.org/10.1016/b978-0-444-53447-7.00075-1
- Barth, N. C., Boulton, C., Carpenter, B. M., Batt, G. E., & Toy, V. G. (2013). Slip localization on the southern Alpine fault, New Zealand. *Tectonics*, 32(3), 620–640. https://doi.org/10.1002/tect.20041
- Barth, N. C., Kulhanek, D. K., Beu, A. G., Murray-Wallace, C. V., Hayward, B. W., Mildenhall, D. C., & Lee, D. E. (2014). New c. 270 kyr strikeslip and uplift rates for the southern Alpine Fault and implications for the New Zealand plate boundary. *Journal of Structural Geology*, 64, 39– 52. https://doi.org/10.1016/j.isg.2013.08.009
- Barth, N. C., Toy, V. G., Langridge, R. M., & Norris, R. J. (2012). Scale dependence of oblique plate-boundary partitioning: New insights from LiDAR, central Alpine fault, New Zealand. Lithosphere, 4(5), 435–448. https://doi.org/10.1130/1201.1
- Batt, G. E., Baldwin, S. L., Cottam, M. A., Fitzgerald, P. G., Brandon, M. T., & Spell, T. L. (2004). Cenozoic plate boundary evolution in the South Island of New Zealand: New thermochronological constraints. *Tectonics*, 23(4), TC4001. https://doi.org/10.1029/2003tc001527
- Batt, G. E., Braun, J., Kohn, B. P., & McDougall, I. (2000). Thermochronological analysis of the dynamics of the Southern Alps, New Zealand. Geological Society of America Bulletin, 112(2), 250–266. https://doi.org/10.1130/0016-7606(2000)112<0250:taotdo>2.3.co;2
- Bea, F. (1996). Residence of REE, Y, Th and U in granites and crustal protoliths; implications for the chemistry of crustal melts. *Journal of Petrology*, 37(3), 521–552. https://doi.org/10.1093/petrology/37.3.521
- Bea, F., Bortnikov, N., Montero, P., Zinger, T., Sharkov, E., Silantyev, S., et al. (2020). Zircon xenocryst evidence for crustal recycling at the Mid-Atlantic Ridge. *Lithos*, 354, 105361. https://doi.org/10.1016/j.lithos.2019.105361
- Bea, F., Morales, I., Molina, J. F., Montero, P., & Cambeses, A. (2021). Zircon stability grids in crustal partial melts: Implications for zircon
- inheritance. Contributions to Mineralogy and Petrology, 176(3), 1–13. https://doi.org/10.1007/s00410-021-01772-x

  Bea, F., Pereira, M. D., & Stroh, A. (1994). Mineral/leucosome trace-element partitioning in a peraluminous migmatite (a laser ablation-ICP-MS study). Chemical Geology, 117(1–4), 291–312. https://doi.org/10.1016/0009-2541(94)90133-3
- Beck, A. C. (1968). Gravity faulting as a mechanism of topographic adjustment. New Zealand Journal of Geology and Geophysics, 11(1), 191–199. https://doi.org/10.1080/00288306.1968.10423684
- Beggs, J. M., & Ghisetti, F. C. (2006). Transpressional structures in Western Southland basins. In New Zealand Petroleum Conference, Wellington, 2006 (pp. 1–9). Crown Ministry of Economic Development
- Wellington, 2006 (pp. 1–9). Crown Minerals, Ministry of Economic Development.

  Belousova, E. A., Griffin, W. L., O'Reilly, S. Y., & Fisher, N. L. (2002). Igneous zircon: Trace element composition as an indicator of source rock
- type. Contributions to Mineralogy and Petrology, 143(5), 602–622. https://doi.org/10.1007/s00410-002-0364-7
  Ben-Zion, Y., & Sammis, C. G. (2003). Characterization of fault zones. Pure and Applied Geophysics, 160, 677–715. https://doi.org/10.1007/978-
- 3-0348-8010-7\_11 Sammis, C. G. (2003). Characterization of fault zones. Pure and Applied Geophysics, 100, 677–715. https://doi.org/10.1007/978
- Berryman, K., Beanland, S., Cooper, A., & Cutten, H. (1992). The Alpine Fault, New Zealand: Quaternary structural style and geomorphic expression. *Annales Tectonicae Special Issue-Supplement to Volume VI*, 126–163.
- Berryman, K. R., Cochran, U. A., Clark, K. J., Biasi, G. P., Langridge, R. M., & Villamor, P. (2012). Major earthquakes occur regularly on an isolated plate boundary fault. *Science*, 336(6089), 1690–1693. https://doi.org/10.1126/science.1218959
- Bhattacharya, S., Kemp, A. I. S., & Collins, W. J. (2018). Response of zircon to melting and metamorphism in deep arc crust, Fiordland (New Zealand): Implications for zircon inheritance in cordilleran granites. Contributions to Mineralogy and Petrology, 173(4), 1–36. https://doi.org/10.1007/s00410-018-1446-5
- Biasi, G. P., & Wesnousky, S. G. (2016). Steps and gaps in ground ruptures: Empirical bounds on rupture propagation. Bulletin of the Seismological Society of America, 106(3), 1110–1124. https://doi.org/10.1785/0120150175
- Biasi, G. P., & Wesnousky, S. G. (2017). Bends and ends of surface ruptures. Bulletin of the Seismological Society of America, 107(6), 2543–2560. https://doi.org/10.1785/0120160292
- Biasi, G. P., & Wesnousky, S. G. (2021). Rupture passing probabilities at fault bends and steps, with application to rupture length probabilities for earthquake early warning. Bulletin of the Seismological Society of America, 111(4), 2235–2247. https://doi.org/10.1785/0120200370
- Black, L. P., Kamo, S. L., Allen, C. M., Davis, D. W., Aleinikoff, J. N., Valley, J. W., et al. (2004). Improved <sup>206</sup>Pb/<sup>238</sup>U microprobe geochronology by the monitoring of a trace-element-related matrix effect; SHRIMP, ID–TIMS, ELA–ICP–MS and oxygen isotope documentation for a series of zircon standards. Chemical Geology, 205(1–2), 115–140. https://doi.org/10.1016/j.chemgeo.2004.01.003
- Blattner, P. (1991). The north Fiordland transcurrent convergence. New Zealand Journal of Geology and Geophysics, 34(4), 533–542. https://doi.org/10.1080/00288306.1991.9514488
- Boese, C. M., Townend, J., Smith, E., & Stern, T. (2012). Microseismicity and stress in the vicinity of the Alpine Fault, central Southern Alps, New Zealand. *Journal of Geophysical Research*, 117(B2), B02302. https://doi.org/10.1029/2011jb008460
- Bolhar, R., Weaver, S. D., Palin, J. M., Cole, J. W., & Paterson, L. A. (2008). Systematics of zircon crystallisation in the Cretaceous Separation Point Suite, New Zealand, using U/Pb isotopes, REE and Ti geothermometry. *Contributions to Mineralogy and Petrology*, 156(2), 133–160. https://doi.org/10.1007/s00410-007-0278-5
- Bovis, M. J. (1982). Uphill-facing (antislope) scarps in the Coast Mountains, southwest British Columbia. *Geological Society of America Bulletin*, 93(8), 804–812. https://doi.org/10.1130/0016-7606(1982)93<804:uasitc>2.0.co;2
- Bradshaw, J. Y. (1990). Geology of crystalline rocks of northern Fiordland: Details of the granulite facies Western Fiordland Orthogneiss and associated rock units. New Zealand Journal of Geology and Geophysics, 33(3), 465–484. https://doi.org/10.1080/00288306.1990.10425702
- Bray, J. D., Seed, R. B., Cluff, L. S., & Seed, H. B. (1994). Earthquake fault rupture propagation through soil. *Journal of Geotechnical Engineering*, 120(3), 543–561. https://doi.org/10.1061/(asce)0733-9410(1994)120:3(543)
- Brophy, J. G. (2008). A study of rare Earth element (REE)–SiO<sub>2</sub> variations in felsic liquids generated by basalt fractionation and amphibolite melting: A potential test for discriminating between the two different processes. *Contributions to Mineralogy and Petrology*, 156(3), 337–357. https://doi.org/10.1007/s00410-008-0289-x
- Cande, S. C., & Stock, J. M. (2004). Pacific—Antarctic—Australia motion and the formation of the Macquarie Plate. Geophysical Journal International, 157(1), 399–414. https://doi.org/10.1111/j.1365-246x.2004.02224.x
- Chamberlain, C. P., Poage, M. A., Craw, D., & Reynolds, R. C. (1999). Topographic development of the Southern Alps recorded by the isotopic composition of authigenic clay minerals, South Island, New Zealand. *Chemical Geology*, 155(3–4), 279–294. https://doi.org/10.1016/s0009-2541(98)00165-x
- Chappell, B. W., & White, A. J. (1974). Two contrasting granite types. Pacific Geology, 8, 489-499.

MERE ET AL. 26 of 34

15252027, 2024, 11, Downloaded from

/agupubs.onlinelibrary.wiley.com/doi/10.1029/2024GC011839, Wiley Online Library on [12/03/2025]. See the Terms

- Chappell, B. W., & White, A. J. (2001). Two contrasting granite types: 25 years later. Australian Journal of Earth Sciences, 48(4), 489–499. https://doi.org/10.1046/j.1440-0952.2001.00882.x
- Childs, C., Manzocchi, T., Walsh, J. J., Bonson, C. G., Nicol, A., & Schöpfer, M. P. (2009). A geometric model of fault zone and fault rock thickness variations. *Journal of Structural Geology*, 31(2), 117–127. https://doi.org/10.1016/j.jsg.2008.08.009
- Claiborne, L. L., Miller, C. F., Walker, B. A., Wooden, J. L., Mazdab, F. K., & Bea, F. (2006). Tracking magmatic processes through Zr/Hf ratios in rocks and Hf and Ti zoning in zircons: An example from the Spirit Mountain batholith, Nevada. *Mineralogical Magazine*, 70(5), 517–543. https://doi.org/10.1180/0026461067050348
- Connelly, J. N. (2001). Degree of preservation of igneous zonation in zircon as a signpost for concordancy in U/Pb geochronology. *Chemical Geology*, 172(1–2), 25–39. https://doi.org/10.1016/s0009-2541(00)00234-5
- Constantine, A. E. (1987). Stratigraphy and Provenance of tertiary sediments at Lake Hauroko, with reference to dextral strike-slip movement on the Moonlight Fault System (Bachelors of Science with Honours Thesis). University of Otago.
- Cooke, M. L., Schottenfeld, M. T., & Buchanan, S. W. (2013). Evolution of fault efficiency at restraining bends within wet kaolin analog experiments. *Journal of Structural Geology*, 51, 180–192. https://doi.org/10.1016/j.jsg.2013.01.010
- Cooper, A. F., Barreiro, B. A., Kimbrough, D. L., & Mattinson, J. M. (1987). Lamprophyre dike intrusion and the age of the Alpine fault, New Zealand. *Geology*, 15(10), 941–944. https://doi.org/10.1130/0091-7613(1987)15<941:ldiata>2.0.co;2
- Corfu, F., Hanchar, J. M., Hoskin, P. W., & Kinny, P. (2003). Atlas of zircon textures. Reviews in Mineralogy and Geochemistry, 53(1), 469–500. https://doi.org/10.2113/0530469
- Cotton, W. R., Fowler, W. L., & Van Velsor, J. E. (1990). Coseismic bedding plane faults and ground fissures associated with the Loma Prieta earthquake of 17 October 1989. In *The Loma Prieta (Santa Cruz Mountains) California, earthquake of 17 October 1989* (Vol. 104, pp. 95–103). California Division of Mines and Geology Special Publications.
- Cowie, P. A., & Scholz, C. H. (1992). Growth of faults by accumulation of seismic slip. *Journal of Geophysical Research*, 97(B7), 11085–11095. https://doi.org/10.1029/92ib00586
- Cox, S. C., & Barrell, D. J. A. (2007). Geology of the Aoraki area, Geological Map. scale 1:250,000 (p. 72). New Zealand Institute of Geological and Nuclear Sciences.
- Cox, S. C., Stirling, M. W., Herman, F., Gerstenberger, M., & Ristau, J. (2012). Potentially active faults in the rapidly eroding landscape adjacent to the Alpine Fault, central Southern Alps, New Zealand. *Tectonics*, 31(2), TC2011. https://doi.org/10.1029/2011tc003038
- Davey, F. J., Eberhart-Phillips, D., Kohler, M. D., Bannister, S., Caldwell, G., Henrys, S., et al. (2007). Geophysical structure of the Southern Alps orogen, South Island, New Zealand. In D. Okaya, T. Stern, & F. Davey (Eds.), A Continental Plate Bounday: Tectonics at South Island, New Zealand, Geophysical Monograph Series (Vol. 175, pp. 47–72). American Geophysical Union. https://doi.org/10.1029/175gm04
- Davey, F. J., Henyey, T., Kleffmann, S., Melhuish, A., Okaya, D. A., Stern, T. A., et al. (1995). Crustal reflections from the Alpine Fault Zone, South Island, New Zealand. New Zealand Journal of Geology and Geophysics, 38(4), 601–604. https://doi.org/10.1080/00288306.1995.
- Davis, K., Burbank, D. W., Fisher, D., Wallace, S., & Nobes, D. (2005). Thrust-fault growth and segment linkage in the active Ostler fault zone, New Zealand. *Journal of Structural Geology*, 27(8), 1528–1546. https://doi.org/10.1016/j.jsg.2005.04.011
- Dawers, N. H., Anders, M. H., & Scholz, C. H. (1993). Growth of normal faults: Displacement-length scaling. *Geology*, 21(12), 1107–1110. https://doi.org/10.1130/0091-7613(1993)021<1107:gonfdl>2.3.co;2
- Dawson, T. E., Weldon, R. J., & Field, E. H. (2013). Appendix B: Geologic slip-rate data and geologic deformation model. US Geological Survey Open-File Report 2013-1165-B. and California Geological Survey Special Report 228-B.
- Decker, M. F. I. (2016). Triggering mechanisms for a magmatic flare-up of the lower crust in Fiordland, New Zealand, from U-Pb zircon geochronology and O-Hf zircon geochemistry (Doctoral dissertation). California State University.
- DeMets, C., & Dixon, T. H. (1999). New kinematic models for Pacific-North America motion from 3 Ma to present, I: Evidence for steady motion and biases in the NUVEL-1A model. *Geophysical Research Letters*, 26(13), 1921–1924. https://doi.org/10.1029/1999g1900405
- DeMets, C., Gordon, R. G., Argus, D. F., & Stein, S. (1994). Effect of recent revisions to the geomagnetic reversal time scale on estimates of current plate motions. *Geophysical Research Letters*, 21(20), 2191–2194. https://doi.org/10.1029/94gl02118
- Dempster, T. J., Hay, D. C., & Bluck, B. J. (2004). Zircon growth in slate. Geology, 32(3), 221–224. https://doi.org/10.1130/g20156.1
- De Pascale, G. P., & Langridge, R. M. (2012). New on-fault evidence for a great earthquake in AD 1717, central Alpine fault, New Zealand. Geology, 40(9), 791–794. https://doi.org/10.1130/g33363.1
- Dolan, J. F., & Haravitch, B. D. (2014). How well do surface slip measurements track slip at depth in large strike-slip earthquakes? The importance of fault structural maturity in controlling on-fault slip versus off-fault surface deformation. *Earth and Planetary Science Letters*, 388, 38–47. https://doi.org/10.1016/j.epsl.2013.11.043
- Dolan, J. F., Van Dissen, R. J., Rhodes, E. J., Zinke, R., Hatem, A. E., McGuire, C., et al. (2024). One tune, many tempos: Faults trade off slip in time and space to accommodate relative plate motions. *Earth and Planetary Science Letters*, 625, 118484. https://doi.org/10.1016/j.epsl.2023. 118484
- Dooley, T., McClay, K., & Bonora, M. (1999). 4D evolution of segmented strike-slip fault systems: Applications to NW Europe. In *Geological Society, London, Petroleum Geology Conference Series* (Vol. 5, No. 1, pp. 215–225). The Geological Society of London. https://doi.org/10.1144/0050215
- Dooley, T. P. (1994). Geometries and kinematics of strike-slip fault systems: Insights from physical modeling and field studies (PhD Thesis). Royal Holloway, University of London.
- Dooley, T. P., & McClay, K. R. (1996). Strike-slip deformation in the Confidence Hills, southern Death Valley fault zone, eastern California, USA. *Journal of the Geological Society*, 153(3), 375–387. https://doi.org/10.1144/gsigs.153.3.0375
- Duan, B., & Oglesby, D. D. (2005). Multicycle dynamics of nonplanar strike-slip faults. *Journal of Geophysical Research*, 110(B3), B03304. https://doi.org/10.1029/2004jb003298
- Eberhart-Phillips, D., Upton, P., Reyners, M., Barrell, D. J., Fry, B., Bourguignon, S., & Warren-Smith, E. (2022). The influence of basement terranes on tectonic deformation: Joint earthquake travel-time and ambient noise tomography of the southern South Island, New Zealand. *Tectonics*, 41(4), e2021TC007006. https://doi.org/10.1029/2021tc007006
- Elliott, A. J., Oskin, M. E., Liu-Zeng, J., & Shao, Y. (2015). Rupture termination at restraining bends: The last great earthquake on the Altyn Tagh fault. Geophysical Research Letters, 42(7), 2164–2170. https://doi.org/10.1002/2015g1063107
- Faulkner, D. R., Jackson, C. A. L., Lunn, R. J., Schlische, R. W., Shipton, Z. K., Wibberley, C. A. J., & Withjack, M. O. (2010). A review of recent developments concerning the structure, mechanics and fluid flow properties of fault zones. *Journal of Structural Geology*, 32(11), 1557–1575. https://doi.org/10.1016/j.jsg.2010.06.009
- Fedorik, J., Maesano, F. E., & Afifi, A. M. (2022). A validated geomechanical model for the strike-slip restraining bend in Lebanon. *Scientific Reports*, 12(1), 20071. https://doi.org/10.1038/s41598-022-24718-0

MERE ET AL. 27 of 34



# Geochemistry, Geophysics, Geosystems

- 10.1029/2024GC011839
- Fink, D., Williams, P., Augustinus, P. C., & Schulmeister, J. (2006). Glacial chronologies across southern hemisphere latitudes during the past 30 ka and correlations to Antarctic ice cores. In P. I. Burge, J. Schulmeister, & C. Turney (Eds.), *Australasian INTIMATE Meeting* (pp. 14–16). University of Auckland.
- Fletcher, J. M., Teran, O. J., Rockwell, T. K., Oskin, M. E., Hudnut, K. W., Mueller, K. J., et al. (2014). Assembly of a large earthquake from a complex fault system: Surface rupture kinematics of the 4 April 2010 El Mayor–Cucapah (Mexico) Mw 7.2 earthquake. *Geosphere*, 10(4), 797–827. https://doi.org/10.1130/ges00933.1
- Fujimaki, H. (1986). Partition coefficients of Hf, Zr, and REE between zircon, apatite, and liquid. Contributions to Mineralogy and Petrology, 94(1), 42–45. https://doi.org/10.1007/bf00371224
- Furlong, K. P., & Kamp, P. J. (2009). The lithospheric geodynamics of plate boundary transpression in New Zealand: Initiating and emplacing subduction along the Hikurangi margin, and the tectonic evolution of the Alpine Fault system. *Tectonophysics*, 474(3–4), 449–462. https://doi. org/10.1016/j.tecto.2009.04.023
- Ghisetti, F. C. (2022). Map-view restorations of the South Island, New Zealand: A reappraisal of the last 10 Myr of evolution of the Alpine and Wairau faults. New Zealand Journal of Geology and Geophysics, 65(2), 336–361. https://doi.org/10.1080/00288306.2021.1878243
- Gibson, G. M. (1982). Stratigraphy and petrography of some metasediments and associated intrusive rocks from central Fiordland, New Zealand. New Zealand Journal of Geology and Geophysics, 25(1), 21–43. https://doi.org/10.1080/00288306.1982.10422503
- Gollan, M. (2006). Plutonic petrogenesis and mineralisation in southwest Fiordland (Masters of Science Thesis). University of Otago.
- Goodman, R. E., & Bray, J. W. (1976). Toppling of rock slopes. In Rock engineering: American Society of Civil Engineers, Geotechnical Engineering Division, Conference, Boulder, Colorado (Vol. 2, pp. 201–237).
- Graham, S. A., Stanley, R. G., Bent, J. V., & Carter, J. B. (1989). Oligocene and Miocene paleogeography of central California and displacement along the San Andreas fault. *Geological Society of America Bulletin*, 101(5), 711–730. https://doi.org/10.1130/0016-7606(1989)101<0711: oampoc>2.3.co;2
- Grimes, C. B., John, B. E., Kelemen, P. B., Mazdab, F. K., Wooden, J. L., Cheadle, M. J., et al. (2007). Trace element chemistry of zircons from oceanic crust: A method for distinguishing detrital zircon provenance. *Geology*, 35(7), 643–646. https://doi.org/10.1130/g23603a.1
- Grimes, C. B., Wooden, J. L., Cheadle, M. J., & John, B. E. (2015). "Fingerprinting" tectono-magmatic provenance using trace elements in igneous zircon. *Contributions to Mineralogy and Petrology*, 170(5–6), 1–26. https://doi.org/10.1007/s00410-015-1199-3
- Hanchar, J. M., & Miller, C. F. (1993). Zircon zonation patterns as revealed by cathodoluminescence and backscattered electron images: Implications for interpretation of complex crustal histories. Chemical Geology, 110(1–3), 1–13. https://doi.org/10.1016/0009-2541(93)90244-d
- Harris, R. A., & Day, S. M. (1999). Dynamic 3D simulations of earthquakes on en echelon faults. Geophysical Research Letters, 26(14), 2089–2092. https://doi.org/10.1029/1999g1900377
- Hatem, A. E., Collett, C. M., Briggs, R. W., Gold, R. D., Angster, S. J., Field, E. H., et al. (2022). Simplifying complex fault data for systems-level analysis: Earthquake geology inputs for US NSHM 2023. Scientific Data, 9(1), 506. https://doi.org/10.1038/s41597-022-01609-7
- Hatem, A. E., Cooke, M. L., & Madden, E. H. (2015). Evolving efficiency of restraining bends within wet kaolin analog experiments. *Journal of Geophysical Research: Solid Earth*, 120(3), 1975–1992. https://doi.org/10.1002/2014jb011735
- Hatem, A. E., Cooke, M. L., & Toeneboehn, K. (2017). Strain localization and evolving kinematic efficiency of initiating strike-slip faults within wet kaolin experiments. *Journal of Structural Geology*, 101, 96–108. https://doi.org/10.1016/j.jsg.2017.06.011
- Hay, D. C., & Dempster, T. J. (2009). Zircon behaviour during low-temperature metamorphism. *Journal of Petrology*, 50(4), 571–589. https://doi.org/10.1093/petrology/egp011
- Heaman, L. M., Bowins, R., & Crocket, J. (1990). The chemical composition of igneous zircon suites: Implications for geochemical tracer studies. Geochimica et Cosmochimica Acta, 54(6), 1597–1607. https://doi.org/10.1016/0016-7037(90)90394-z
- Herman, F., Cox, S. C., & Kamp, P. J. (2009). Low-temperature thermochronology and thermokinematic modeling of deformation, exhumation, and development of topography in the central Southern Alps, New Zealand. *Tectonics*, 28(5), TC5011. https://doi.org/10.1029/2008tc002367
- Hiess, J., Ireland, T., & Rattenbury, M. (2010). U-Th-Pb zircon and monazite geochronology of Western Province gneissic rocks, central-south Westland. New Zealand. New Zealand Journal of Geology and Geophysics. 53(4), 241–269. https://doi.org/10.1080/00288306.2010.495450
- Hiess, J., Yi, K., Woodhead, J., Ireland, T., & Rattenbury, M. (2015). Gondwana margin evolution from zircon REE, O and Hf signatures of Western Province gneisses, Zealandia. Geological Society, London, Special Publications, 389(1), 323–353. https://doi.org/10.1144/sp389.10
- Hollis, J. A., Clarke, G. L., Klepeis, K. A., Daczko, N. R., & Ireland, T. R. (2003). Geochronology and geochemistry of high-pressure granulites of the Arthur River Complex, Fiordland, New Zealand: Cretaceous magmatism and metamorphism on the palaeo-Pacific Margin. *Journal of Metamorphic Geology*, 21(3), 299–313. https://doi.org/10.1046/j.1525-1314.2003.00443.x
- Hollis, J. A., Clarke, G. L., Klepeis, K. A., Daczko, N. R., & Ireland, T. R. (2004). The regional significance of Cretaceous magmatism and metamorphism in Fiordland, New Zealand, from U–Pb zircon geochronology. *Journal of Metamorphic Geology*, 22(7), 607–627. https://doi.org/10.1111/j.1525-1314.2004.00537.x
- Hoskin, P. W., & Ireland, T. R. (2000). Rare Earth element chemistry of zircon and its use as a provenance indicator. *Geology*, 28(7), 627–630. https://doi.org/10.1130/0091-7613(2000)028<0627;recoz>2.3.co;2
- Hoskin, P. W. O., & Black, L. P. (2000). Metamorphic zircon formation by solid-state recrystallization of protolith igneous zircon. *Journal of Metamorphic Geology*, 18(4), 423–439. https://doi.org/10.1046/j.1525-1314.2000.00266.x
- Hout, C., Stowell, H., Schwartz, J., & Klepeis, K. (2012). New <sup>206</sup>Pb/<sup>238</sup>U zircon ages record magmatism and metamorphism in the crustal root of a magmatic arc, Fiordland, New Zealand. In *Geological Society of America Abstracts with Programs* (Vol. 44, No. 7, p. 586).
- Howarth, J. D., Barth, N. C., Fitzsimons, S. J., Richards-Dinger, K., Clark, K. J., Biasi, G. P., et al. (2021). Spatiotemporal clustering of great earthquakes on a transform fault controlled by geometry. *Nature Geoscience*, 14(5), 314–320. https://doi.org/10.1038/s41561-021-00721-4
- Howarth, J. D., Cochran, U. A., Langridge, R. M., Clark, K., Fitzsimons, S. J., Berryman, K., et al. (2018). Past large earthquakes on the Alpine Fault: Paleoseismological progress and future directions. New Zealand Journal of Geology and Geophysics, 61(3), 309–328. https://doi.org/10. 1080/00288306.2018.1464658
- Hull, A. G., & Berryman, K. R. (1986). Holocene tectonism in the region of the Alpine fault at Lake McKerrow, Fiordland, New Zealand. *Recent Crustal Movements of the Pacific Region*, 24, 317–331.
- Hunt, T. (1978). Stokes magnetic anomaly system. New Zealand Journal of Geology and Geophysics, 21(5), 595–606. https://doi.org/10.1080/00288306.1978.10424087
- Irel, T. R., & Gibson, G. M. (1998). SHRIMP monazite and zircon geochronology of high-grade metamorphism in New Zealand. *Journal of Metamorphic Geology*, 16(2), 149–167. https://doi.org/10.1111/j.1525-1314.1998.00112.x
- Ireland, T. R. (1992). Crustal evolution of New Zealand: Evidence from age distributions of detrital zircons in Western Province paragneisses and Torlesse greywacke. *Geochimica et Cosmochimica Acta*, 56(3), 911–920. https://doi.org/10.1016/0016-7037(92)90036-i
- Jackson, S. E., Pearson, N. J., Griffin, W. L., & Belousova, E. A. (2004). The application of laser ablation-inductively coupled plasma-mass spectrometry to in situ U-Pb zircon geochronology. Chemical Geology, 211(1-2), 47-69. https://doi.org/10.1016/j.chemgeo.2004.06.017

MERE ET AL. 28 of 34

15252027, 2024, 11, Downloaded from

online library wiley com/doi/10.1029/2024GC011839, Wiley Online Library on [12/03/2025]. See the Terms and Conditions

- Jaffey, A. H., Flynn, K. F., Glendenin, L. E., Bentley, W. T., & Essling, A. M. (1971). Precision measurement of half-lives and specific activities of <sup>235</sup>U and <sup>238</sup>U. *Physical Review C*, 4(5), 1889–1906. https://doi.org/10.1103/physrevc.4.1889
- Jara, J. J., Barra, F., Reich, M., Leisen, M., Romero, R., & Morata, D. (2021). Episodic construction of the early Andean Cordillera unravelled by zircon petrochronology. Nature Communications, 12(1), 4930. https://doi.org/10.1038/s41467-021-25232-z
- Johnston, M. R. (1990). Geology of the St. Arnaud District, Southeast Nelson (Sheet N29). New Zealand Geological Survey Bulletin, 99(119), 112–115.
- Kamp, P. J. (1986). The mid-Cenozoic Challenger Rift System of western New Zealand and its implications for the age of Alpine fault inception. Geological Society of America Bulletin, 97(3), 255–281. https://doi.org/10.1130/0016-7606(1986)97<255:tmcrso>2.0.co;2
- Kamp, P. J., Green, P. F., & Tippett, J. M. (1992). Tectonic architecture of the mountain front-foreland basin transition, South Island, New Zealand, assessed by fission track analysis. *Tectonics*, 11(1), 98–113. https://doi.org/10.1029/91tc02362
- Kelemen, P. B., Hanghøj, K., & Greene, A. R. (2014). One view of the geochemistry of subduction-related magmatic arcs, with an emphasis on primitive andesite and lower crust. Elsevier.
- Kennedy, A. K., Wotzlaw, J. F., Schaltegger, U., Crowley, J. L., & Schmitz, M. (2014). Eocene zircon reference material for microanalysis of U-Th-Pb isotopes and trace elements. *The Canadian Mineralogist*, 52(3), 409–421. https://doi.org/10.3749/canmin.52.3.409
- Khajavi, N., Quigley, M., & Langridge, R. M. (2014). Influence of topography and basement depth on surface rupture morphology revealed from LiDAR and field mapping, Hope Fault, New Zealand. *Tectonophysics*, 630, 265–284. https://doi.org/10.1016/j.tecto.2014.05.032
- Kim, Y. S., & Sanderson, D. J. (2006). Structural similarity and variety at the tips in a wide range of strike–slip faults: A review. *Terra Nova*, 18(5), 330–344. https://doi.org/10.1111/j.1365-3121.2006.00697.x
- Kimbrough, D. L., Tulloch, A. J., Coombs, D. S., Landis, C. A., Johnston, M. R., & Mattinson, J. M. (1994). Uranium-lead zircon ages from the median tectonic zone, New Zealand. New Zealand Journal of Geology and Geophysics, 37(4), 393–419. https://doi.org/10.1080/00288306. 1994 9514630
- Kimbrough, D. L., Tulloch, A. J., Geary, E., Coombs, D. S., & Landis, C. A. (1993). Isotopic ages from the Nelson region of South Island New Zealand: Crustal structure and definition of the Median Tectonic Zone. *Tectonophysics*, 225(4), 433–448. https://doi.org/10.1016/0040-1951 (93)90308-7
- King, D. S., Klepeis, K. A., Goldstein, A. G., Gehrels, G. E., & Clarke, G. L. (2008). The initiation and evolution of the transpressional Straight River shear zone, central Fiordland, New Zealand. *Journal of Structural Geology*, 30(4), 410–430. https://doi.org/10.1016/j.jsg.2007.12.004
- King, P. R. (2000). Tectonic reconstructions of New Zealand: 40 Ma to the present. New Zealand Journal of Geology and Geophysics, 43(4), 611–638. https://doi.org/10.1080/00288306.2000.9514913
- Klepeis, K. A., Clarke, G. L., Gehrels, G., & Vervoort, J. (2004). Processes controlling vertical coupling and decoupling between the upper and lower crust of orogens: Results from Fiordland, New Zealand. *Journal of Structural Geology*, 26(4), 765–791. https://doi.org/10.1016/j.jsg. 2003.08.012
- Klepeis, K. A., Daczko, N. R., & Clarke, G. L. (1999). Kinematic vorticity and tectonic significance of superposed mylonites in a major lower crustal shear zone, northern Fiordland, New Zealand. *Journal of Structural Geology*, 21(10), 1385–1405. https://doi.org/10.1016/s0191-8141
- Klepeis, K. A., Schwartz, J., Stowell, H., & Tulloch, A. (2016). Gneiss domes, vertical and horizontal mass transfer, and the initiation of extension in the hot lower-crustal root of a continental arc, Fiordland, New Zealand. Lithosphere, 8(2), 116–140. https://doi.org/10.1130/1490.1
- Klepeis, K. A., Webb, L. E., Blatchford, H. J., Jongens, R., Turnbull, R. E., & Schwartz, J. J. (2019). The age and origin of Miocene-Pliocene fault reactivations in the upper plate of an incipient subduction zone, Puysegur Margin, New Zealand. *Tectonics*, 38(8), 3237–3260. https://doi.org/ 10.1029/2019tc005674
- Klepeis, K. A., Webb, L. E., Blatchford, H. J., Schwartz, J., Jongens, R., Turnbull, R., & Stowell, H. (2019). Deep slab collision during Miocene subduction causes uplift along crustal-scale reverse faults in Fiordland, New Zealand. Geological Society of America Today, 29(9), 4–10. https://doi.org/10.1130/gsatg399a.1
- Kokalj, Ž., & Somrak, M. (2019). Why not a single image? Combining visualizations to facilitate fieldwork and on-screen mapping. *Remote Sensing*, 11(7), 747. https://doi.org/10.3390/rs11070747
- Koons, P. O., Norris, R. J., Craw, D., & Cooper, A. F. (2003). Influence of exhumation on the structural evolution of transpressional plate boundaries: An example from the Southern Alps, New Zealand. *Geology*, 31(1), 3–6. https://doi.org/10.1130/0091-7613(2003)031<0003:
- Korup, O. (2004). Geomorphic implications of fault zone weakening: Slope instability along the Alpine Fault, South Westland to Fiordland. New Zealand Journal of Geology and Geophysics, 47(2), 257–267. https://doi.org/10.1080/00288306.2004.9515052
- Kylander-Clark, A. R., Hacker, B. R., & Cottle, J. M. (2013). Laser-ablation split-stream ICP petrochronology. Chemical Geology, 345, 99–112. https://doi.org/10.1016/j.chemgeo.2013.02.019
- Lamarche, G., & Lebrun, J. F. (2000). Transition from strike-slip faulting to oblique subduction: Active tectonics at the Puysegur Margin, South New Zealand. *Tectonophysics*, 316(1–2), 67–89. https://doi.org/10.1016/s0040-1951(99)00232-2
- Lamb, S. (2011). Cenozoic tectonic evolution of the New Zealand plate-boundary zone: A paleomagnetic perspective. *Tectonophysics*, 509(3–4), 135–164. https://doi.org/10.1016/j.tecto.2011.06.005
- Lamb, S., & Mortimer, N. (2021). Taking time to twist a continent—Multistage origin of the New Zealand orocline. Geology, 49(1), 56–60. https://doi.org/10.1130/g47805.1
- Lamb, S., Mortimer, N., Smith, E., & Turner, G. (2016). Focusing of relative plate motion at a continental transform fault: Cenozoic dextral displacement> 700 km on New Zealand's Alpine Fault, reversing> 225 km of Late Cretaceous sinistral motion. *Geochemistry, Geophysics, Geosystems*, 17(3), 1197–1213. https://doi.org/10.1002/2015gc006225
- Lamb, S., Smith, E., Stern, T., & Warren-Smith, E. (2015). Continent-scale strike-slip on a low-angle fault beneath NewZ ealand's Southern Alps: Implications for crustal thickening in oblique collision zones. *Geochemistry, Geophysics, Geosystems*, 16(9), 3076–3096. https://doi.org/10. 1002/2015sc005990
- Langridge, R. M., Ries, W. F., Farrier, T., Barth, N. C., Khajavi, N., & De Pascale, G. P. (2014). Developing sub 5-m LiDAR DEMs for forested sections of the Alpine and Hope faults, South Island, New Zealand: Implications for structural interpretations. *Journal of Structural Geology*, 64, 53–66. https://doi.org/10.1016/j.jsg.2013.11.007
- Langridge, R. M., Ries, W. F., Litchfield, N. J., Villamor, P., Van Dissen, R. J., Barrell, D. J. A., et al. (2016). The New Zealand active faults database. New Zealand Journal of Geology and Geophysics, 59(1), 86–96. https://doi.org/10.1080/00288306.2015.1112818
- Lebrun, J. F., Lamarche, G., & Collot, J. Y. (2003). Subduction initiation at a strike-slip plate boundary: The Cenozoic Pacific-Australian plate boundary, south of New Zealand. *Journal of Geophysical Research*, 108(B9), 2453. https://doi.org/10.1029/2002jb002041
- Lebrun, J. F., Lamarche, G., Collot, J. Y., & Delteil, J. (2000). Abrupt strike-slip fault to subduction transition: The Alpine fault-Puysegur trench connection, New Zealand. *Tectonics*, 19(4), 688–706. https://doi.org/10.1029/2000tc900008

MERE ET AL. 29 of 34



- Leitner, B., Eberhart-Phillips, D., Anderson, H., & Nabelek, J. L. (2001). A focused look at the Alpine fault, New Zealand: Seismicity, focal mechanisms, and stress observations. *Journal of Geophysical Research*, 106(B2), 2193–2220. https://doi.org/10.1029/2000jb900303
- Litchfield, N. J., Van Dissen, R., Sutherland, R., Barnes, P. M., Cox, S. C., Norris, R., et al. (2014). A model of active faulting in New Zealand. New Zealand Journal of Geology and Geophysics, 57(1), 32–56. https://doi.org/10.1080/00288306.2013.854256
- Litchfield, N. J., Villamor, P., Dissen, R. J. V., Nicol, A., Barnes, P. M., A. Barrell, D. J., et al. (2018). Surface rupture of multiple crustal faults in the 2016 M w 7.8 Kaikōura, New Zealand, Earthquake. Bulletin of the Seismological Society of America, 108(3B), 1496–1520. https://doi.org/ 10.1785/0120170300
- Little, T. A., Cox, S., Vry, J. K., & Batt, G. (2005). Variations in exhumation level and uplift rate along the oblique-slip Alpine fault, central Southern Alps, New Zealand. *Geological Society of America Bulletin*, 117(5–6), 707–723. https://doi.org/10.1130/b25500.1
- Little, T. A., & Jones, A. (1998). Seven million years of strike-slip and related off-fault deformation, northeastern Marlborough fault system, South Island, New Zealand. Tectonics, 17(2), 285–302. https://doi.org/10.1029/97tc03148
- Lozos, J. C. (2021). The effect of along-strike variation in dip on rupture propagation on strike-slip faults. Geosphere, 17(6), 1616–1630. https://doi.org/10.1130/ges02391.1
- Lozos, J. C., Oglesby, D. D., Duan, B., & Wesnousky, S. G. (2011). The effects of double fault bends on rupture propagation: A geometrical parameter study. *Bulletin of the Seismological Society of America*, 101(1), 385–398. https://doi.org/10.1785/0120100029
- Ludwig, K. R. (2009). Isoplot v. 4 for Excel 2007. Berkeley Geochronology Center.
- Lukács, A., Gorman, A. R., & Norris, R. J. (2019). Quaternary structural and paleo-environmental evolution of the Alpine Fault near Haast, New Zealand, from 2D seismic reflection and gravity data. New Zealand Journal of Geology and Geophysics, 62(2), 229–247. https://doi.org/10.1080/00288306.2018.1544153
- Manighetti, I., Campillo, M., Bouley, S., & Cotton, F. (2007). Earthquake scaling, fault segmentation, and structural maturity. Earth and Planetary Science Letters, 253(3-4), 429-438. https://doi.org/10.1016/j.epsl.2006.11.004
- Manighetti, I., King, G., & Sammis, C. G. (2004). The role of off-fault damage in the evolution of normal faults. Earth and Planetary Science Letters, 217(3–4), 399–408. https://doi.org/10.1016/s0012-821x(03)00601-0
- Manighetti, I., Mercier, A., & De Barros, L. (2021). Fault trace corrugation and segmentation as a measure of fault structural maturity. Geophysical Research Letters, 48(20), e2021GL095372. https://doi.org/10.1029/2021gl095372
- Mann, P. (2007). Global catalogue, classification and tectonic origins of restraining-and releasing bends on active and ancient strike-slip fault systems. Geological Society, London, Special Publications, 290(1), 13–142. https://doi.org/10.1144/sp290.2
- Mann, P., & Gordon, M. B. (1996). Tectonic uplift and exhumation of blueschist belts along transpressional strike-slip fault zones. *Geophysical Managraph-American Geophysical Union* 96, 143–154. https://doi.org/10.1029/cm096n0143
- Monograph-American Geophysical Union, 96, 143–154. https://doi.org/10.1029/gm096p0143

  Marshall, S., Plesch, A., & Shaw, J. (2023). SCEC Community Fault Model (CFM) version 6.0. Retrieved from https://zenodo.org/record/
- 7809330
  Matti, J. C., & Morton, D. M. (1993). Paleogeographic evolution of the San Andreas fault in southern California: A reconstruction based on a new
- cross-fault correlation.

  McCalpin, J. P. (1999). Criteria for determining the seismic significance of sackungen and other scarplike landforms in mountainous regions, Techniques for identifying faults and determining their origins (pp. 2–55). US Nuclear Regulatory Commission.
- McClay, K., & Bonora, M. (2001). Analog models of restraining stepovers in strike-slip fault systems. AAPG Bulletin, 85(2), 233–260. https://doi.org/10.1306/8626c7ad-173b-11d7-8645000102c1865d
- McCoy-West, A. J., Mortimer, N., & Ireland, T. R. (2014). U–Pb geochronology of Permian plutonic rocks, Longwood Range, New Zealand: Implications for Median Batholith–Brook Street Terrane relations. New Zealand Journal of Geology and Geophysics, 57(1), 65–85. https://doi.org/10.1080/00288306.2013.869235
- Melhuish, A., Sutherland, R., Davey, F. J., & Lamarche, G. (1999). Crustal structure and neotectonics of the Puysegur oblique subduction zone, New Zealand. *Tectonophysics*, 313(4), 335–362. https://doi.org/10.1016/s0040-1951(99)00212-7
- Mere, A. M., & Barth, N. C. (2024). Active fault traces of the southern Alpine Fault Zone, New Zealand. Zenodo. https://doi.org/10.5281/zenodo.
- Mere, A. M., & McPhillips, D. (2024). Fault activity in the San Gabriel Mountains, southern California, USA: Insights from landscape morphometrics, erosion rates, and fault-slip rates. *Geological Society of America Bulletin*, 136(7–8), 3353–3376. https://doi.org/10.1130/b37218.1
- Mitra, S., & Paul, D. (2011). Structural geometry and evolution of releasing and restraining bends: Insights from laser-scanned experimental models. AAPG Bulletin, 95(7), 1147–1180. https://doi.org/10.1306/09271010060
- Mortimer, N. (2014). The oroclinal bend in the South Island, New Zealand. *Journal of Structural Geology*, 64, 32–38. https://doi.org/10.1016/j.jsg.2013.08.011
- Mortimer, N. (2018). Evidence for a pre-Eocene proto-Alpine Fault through Zealandia. New Zealand Journal of Geology and Geophysics, 61(3), 251–259. https://doi.org/10.1080/00288306.2018.1434211
- Mortimer, N., Nathan, S., Jongens, R., Kawachi, Y., Ryland, C., Cooper, A. F., et al. (2013). Regional metamorphism of the Early Palaeozoic Greenland Group, South Westland, New Zealand. New Zealand Journal of Geology and Geophysics, 56(1), 1–15. https://doi.org/10.1080/00288306.2012.734830
- Mortimer, N., Rattenbury, M., King, P., Bland, K., Barrell, D., Bache, F., et al. (2014). High-level stratigraphic scheme for New Zealand rocks. New Zealand Journal of Geology and Geophysics, 57(4), 402–419. https://doi.org/10.1080/00288306.2014.946062
- Muir, R. J., Ireland, T. R., Weaver, S. D., & Bradshaw, J. D. (1994). Ion microprobe U Pb zircon geochronology of granitic magmatism in the Western Province of the South Island, New Zealand. Chemical Geology, 113(1–2), 171–189. https://doi.org/10.1016/0009-2541(94)90011-6
- Muir, R. J., Ireland, T. R., Weaver, S. D., & Bradshaw, J. D. (1996). Ion microprobe dating of Paleozoic granitoids: Devonian magmatism in New Zealand and correlations with Australia and Antarctica. *Chemical Geology*, 127(1–3), 191–210. https://doi.org/10.1016/0009-2541(95) 00092-5
- Muir, R. J., Ireland, T. R., Weaver, S. D., Bradshaw, J. D., Evans, J. A., Eby, G. N., & Shelley, D. (1998). Geochronology and geochemistry of a Mesozoic magmatic arc system, Fiordland, New Zealand. *Journal of the Geological Society*, 155(6), 1037–1053. https://doi.org/10.1144/gsjgs. 155.6.1037
- Muir, R. J., Ireland, T. R., Weaver, S. D., Bradshaw, J. D., Waight, T. E., Jongens, R., & Eby, G. N. (1997). SHRIMP U-Pb geochronology of Cretaceous magmatism in northwest Nelson-Westland, South Island, New Zealand. New Zealand Journal of Geology and Geophysics, 40(4), 453–463. https://doi.org/10.1080/00288306.1997.9514775
- Müller, R. D., Zahirovic, S., Williams, S. E., Cannon, J., Seton, M., Bower, D. J., et al. (2019). A global plate model including lithospheric deformation along major rifts and orogens since the Triassic. *Tectonics*, 38(6), 1884–1907. https://doi.org/10.1029/2018tc005462

MERE ET AL. 30 of 34

5252027, 2024, 11, Downloaded from https

onlinelibrary.wiley.com/doi/10.1029/2024GC011839, Wiley Online Library on [12/03/2025]. See the Terms

- Nardi, L. V. S., Formoso, M. L. L., Müller, I. F., Fontana, E., Jarvis, K., & Lamarão, C. (2013). Zircon/rock partition coefficients of REEs, Y, Th, U, Nb, and Ta in granitic rocks: Uses for provenance and mineral exploration purposes. *Chemical Geology*, 335, 1–7. https://doi.org/10.1016/j.chemgeo.2012.10.043
- Nathan, S. (1978). Upper Cenozoic stratigraphy of South Westland, New Zealand. New Zealand Journal of Geology and Geophysics, 21(3), 329–361. https://doi.org/10.1080/00288306.1978.10424061
- Nathan, S., Rattenbury, M. S., & Suggate, R. P. (2002). Geology of the Greymouth Area, Geological Map 9. scale 1:250,000 (p. 58). New Zealand Institute of Geological and Nuclear Sciences.
- Naylor, M. A., Mandl, G. T., & Supesteijn, C. H. K. (1986). Fault geometries in basement-induced wrench faulting under different initial stress states. *Journal of Structural Geology*, 8(7), 737–752. https://doi.org/10.1016/0191-8141(86)90022-2
- Nevitt, J. M., Brooks, B. A., Hardebeck, J. L., & Aagaard, B. T. (2023). 2019 M7. 1 Ridgecrest earthquake slip distribution controlled by fault geometry inherited from Independence dike swarm. *Nature Communications*, 14(1), 1546. https://doi.org/10.1038/s41467-023-36840-2
- Newsome, P. F. J. (1987). The vegetative cover of New Zealand (water and soil miscellaneous publication No. 112). Water and Soil Directorate, Ministry of Works and Development.
- Norris, R. J., & Carter, R. M. (1980). Offshore sedimentary basins at the southern end of the Alpine Fault, New Zealand, Sedimentation in oblique-slip mobile zones (pp. 237–265).
- Norris, R. J., & Cooper, A. F. (1995). Origin of small-scale segmentation and transpressional thrusting along the Alpine fault, New Zealand. Geological Society of America Bulletin, 107(2), 231–240. https://doi.org/10.1130/0016-7606(1995)107<0231:oosssa>2.3.co;2
- Norris, R. J., & Cooper, A. F. (1997). Erosional control on the structural evolution of a transpressional thrust complex on the Alpine Fault, New Zealand. *Journal of Structural Geology*, 19(10), 1323–1342. https://doi.org/10.1016/s0191-8141(97)00036-9
- Norris, R. J., & Cooper, A. F. (2001). Late Quaternary slip rates and slip partitioning on the Alpine Fault, New Zealand. *Journal of Structural Geology*, 23(2–3), 507–520. https://doi.org/10.1016/s0191-8141(00)00122-x
- Norris, R. J., & Cooper, A. F. (2003). Very high strains recorded in mylonites along the Alpine Fault, New Zealand: Implications for the deep structure of plate boundary faults. *Journal of Structural Geology*, 25(12), 2141–2157. https://doi.org/10.1016/s0191-8141(03)00045-2
- Norris, R. J., & Cooper, A. F. (2007). The Alpine Fault, New Zealand: Surface geology and field relationships. In D. Okaya, T. Stern, & F. Davey (Eds.), A Continental Plate Bounday: Tectonics at South Island, New Zealand, Geophysical Monograph Series (Vol. 175, pp. 157–175). American Geophysical Union. https://doi.org/10.1029/175gm09
- Norris, R. J., Koons, P. O., & Cooper, A. F. (1990). The obliquely-convergent plate boundary in the South Island of New Zealand: Implications for ancient collision zones. *Journal of Structural Geology*, 12(5–6), 715–725. https://doi.org/10.1016/0191-8141(90)90084-c
- Norris, R. J., & Toy, V. G. (2014). Continental transforms: A view from the Alpine Fault. *Journal of Structural Geology*, 64, 3–31. https://doi.org/10.1016/j.jsg.2014.03.003
- Norris, R. J., & Turnbull, I. M. (1993). Cenozoic basins adjacent to an evolving transform plate boundary, southwest New Zealand, South Pacific Sedimentary Basins. Sedimentary Basins of the World (Vol. 2, pp. 251–270). Elsevier Science Publishers.
- Oliver, G. J. H., & Coggon, J. H. (1979). Crustal structure of Fiordland, New Zealand. *Tectonophysics*, 54(3–4), 253–292. https://doi.org/10.1016/
- Oskin, M. E., Arrowsmith, J. R., Corona, A. H., Elliott, A. J., Fletcher, J. M., Fielding, E. J., et al. (2012). Near-field deformation from the El Mayor–Cucapah earthquake revealed by differential LIDAR. *Science*, 335(6069), 702–705. https://doi.org/10.1126/science.1213778
- Peacock, D. C. P., & Sanderson, D. J. (1991). Displacements, segment linkage and relay ramps in normal fault zones. *Journal of Structural Geology*, 13(6), 721–733. https://doi.org/10.1016/0191-8141(91)90033-f
- Pearson, K. (1901). LIII. On lines and planes of closest fit to systems of points in space. The London, Edinburgh and Dublin Philosophical Magazine and Journal of Science, 2(11), 559–572. https://doi.org/10.1080/14786440109462720
- Perrin, C., Manighetti, I., Ampuero, J. P., Cappa, F., & Gaudemer, Y. (2016). Location of largest earthquake slip and fast rupture controlled by along-strike change in fault structural maturity due to fault growth. *Journal of Geophysical Research: Solid Earth*, 121(5), 3666–3685. https://doi.org/10.1002/2015ib012671
- Ponti, D. J., & Wells, R. E. (1991). Off-fault ground ruptures in the Santa Cruz Mountains, California: Ridge-top spreading versus tectonic extension during the 1989 Loma Prieta earthquake. *Bulletin of the Seismological Society of America*, 81(5), 1480–1510.
- Putnam, A. E., Schaefer, J. M., Barrell, D. J. A., Vandergoes, M., Denton, G. H., Kaplan, M. R., et al. (2010). In situ cosmogenic <sup>10</sup>Be production-rate calibration from the Southern Alps, New Zealand. *Quaternary Geochronology*, 5(4), 392–409. https://doi.org/10.1016/j.quageo.2009.
- Putnam, A. E., Schaefer, J. M., Denton, G. H., Barrell, D. J., Birkel, S. D., Andersen, B. G., et al. (2013). The last glacial maximum at 44°S documented by a <sup>10</sup>Be moraine chronology at Lake Ohau, Southern Alps of New Zealand. *Quaternary Science Reviews*, 62, 114–141. https://doi.org/10.1016/j.quascirev.2012.10.034
- Quigley, M., Van Dissen, R., Litchfield, N., Villamor, P., Duffy, B., Barrell, D., et al. (2012). Surface rupture during the 2010 M<sub>w</sub> 7.1 Darfield (Canterbury) earthquake: Implications for fault rupture dynamics and seismic-hazard analysis. *Geology*, 40(1), 55–58. https://doi.org/10.1130/g32528.1
- Rahe, B., Ferrill, D. A., & Morris, A. P. (1998). Physical analog modeling of pull-apart basin evolution. *Tectonophysics*, 285(1–2), 21–40. https://doi.org/10.1016/s0040-1951(97)00193-5
- Ramezani, J., & Tulloch, A. J. (2009). TIMS U-Pb geochronology of southern and eastern Fiordland. Techfile Report: QMap Fiordland.
- Rattenbury, M. S., Jongens, R., & Cox, S. C. (2010). Geology of the Haast area, Geological Map 14. scale 1:250,000 (p. 61). New Zealand Institute of Geological and Nuclear Sciences.
- Rattenbury, M. S., A, C. R., & Johnston, M. R. (1998). Geology of the Nelson Area. New Zealand Institute of Geological and Nuclear Sciences. scale 1:250,000.
- Reid, H. F. (1910). The mechanism of the earthquake, the California earthquake of April 18, 1906, Report of the Research Senatorial Commission (Vol. 2, pp. 16–18). Carnegie Institution.
- Richard, P. D., Naylor, M. A., & Koopman, A. (1995). Experimental models of strike-slip tectonics. *Petroleum Geoscience*, *I*(1), 71–80. https://doi.org/10.1144/petgeo.1.1.71
- Ring, U., Glodny, J., Angiboust, S., Little, T., & Lang, K. A. (2019). Middle to Late Miocene age for the end of amphibolite-facies mylonitization of the Alpine Schist, New Zealand: Implications for onset of transpression across the Alpine Fault. *Tectonics*, 38(12), 4335–4359. https://doi.org/10.1029/2019tc005577
- Rodriguez Padilla, A. M., Oskin, M. E., Milliner, C. W., & Plesch, A. (2022). Accrual of widespread rock damage from the 2019 Ridgecrest earthquakes. *Nature Geoscience*, 15(3), 222–226. https://doi.org/10.1038/s41561-021-00888-w
- Rubatto, D. (2017). Zircon: The metamorphic mineral. Reviews in Mineralogy and Geochemistry, 83(1), 261–295. https://doi.org/10.2138/rmg\_2017.83.9

MERE ET AL. 31 of 34

15252027, 2024, 11, Downloaded from

onlinelibrary.wiley.com/doi/10.1029/2024GC011839, Wiley Online Library on [12/03/2025]. See the Terms

- Rubatto, D., & Gebauer, D. (2000). Use of cathodoluminescence for U-Pb zircon dating by ion microprobe: Some examples from the Western Alps. In *Cathodoluminescence in geosciences* (pp. 373–400). Springer Berlin Heidelberg.
- Rubatto, D., & Hermann, J. (2007). Experimental zircon/melt and zircon/garnet trace element partitioning and implications for the geochronology of crustal rocks. *Chemical Geology*, 241(1–2), 38–61. https://doi.org/10.1016/j.chemgeo.2007.01.027
- Ryland, C. B. (2011). The geology and structural evolution of the bald Hill-Maori saddle region, South Westland, New Zealand (PhD dissertation). University of Otago.
- Sagar, M. W., Palin, J. M., Tulloch, A. J., & Heath, L. A. (2016). The geology, geochronology and affiliation of the Glenroy Complex and adjacent plutonic rocks, southeast Nelson. *New Zealand Journal of Geology and Geophysics*, *59*(2), 213–235. https://doi.org/10.1080/00288306.2015.
- Schaltegger, U., Fanning, C. M., Günther, D., Maurin, J. C., Schulmann, K., & Gebauer, D. (1999). Growth, annealing and recrystallization of zircon and preservation of monazite in high-grade metamorphism: Conventional and in-situ U-Pb isotope, cathodoluminescence and microchemical evidence. Contributions to Mineralogy and Petrology, 134(2-3), 186-201. https://doi.org/10.1007/s004100050478
- Scholz, C. H., Ando, R., & Shaw, B. E. (2010). The mechanics of first order splay faulting: The strike-slip case. *Journal of Structural Geology*, 32(1), 118–126. https://doi.org/10.1016/j.jsg.2009.10.007
- Scholz, C. H., & Lawler, T. M. (2004). Slip tapers at the tips of faults and earthquake ruptures. *Geophysical Research Letters*, 31(21), L21609. https://doi.org/10.1029/2004gl021030
- Schwartz, J., Brackman, A., Carty, K., Greenberg, G., Klepeis, K. A., Stowell, H. H., & Barnes, C. (2021). The diversification of cordilleran arc melts in the deep crust of Fiordland, New Zealand. In *Geological Society of America Abstracts with Programs*.
- Schwartz, J. J., Klepeis, K. A., Sadorski, J. F., Stowell, H. H., Tulloch, A. J., & Coble, M. A. (2017). The tempo of continental arc construction in the Mesozoic Median Batholith, Fiordland, New Zealand. *Lithosphere*, 9(3), 343–365. https://doi.org/10.1130/1610.1
- Schwartz, J. J., Stowell, H. H., Klepeis, K. A., Tulloch, A. J., Kylander-Clark, A. R., Hacker, B. R., & Coble, M. A. (2016). Thermochronology of extensional orogenic collapse in the deep crust of Zealandia. *Geosphere*, 12(3), 647–677. https://doi.org/10.1130/ges01232.1
- Scott, J. M., & Palin, J. M. (2008). LA-ICP-MS U-Pb zircon ages from Mesozoic plutonic rocks in eastern Fiordland, New Zealand. New Zealand Journal of Geology and Geophysics, 51(2), 105–113. https://doi.org/10.1080/00288300809509853
- Scott, J. M., Turnbull, I. M., Ewing, T. A., Allibone, A. H., Palin, J. M., & Cooper, A. F. (2008). Petrology and geochronology of the volcaniclastic and volcanogenic Mesozoic Loch Burn Formation in eastern Fiordland, New Zealand. New Zealand Journal of Geology and Geophysics, 51(2), 89–103. https://doi.org/10.1080/00288300809509852
- Seebeck, H., Van Dissen, R., Litchfield, N., Barnes, P. M., Nicol, A., Langridge, R., et al. (2024). The New Zealand Community Fault Model-version 1.0: An improved geological foundation for seismic hazard modelling. New Zealand Journal of Geology and Geophysics, 67(2), 209–229. https://doi.org/10.1080/00288306.2023.2181362
- Seward, D., & Nathan, S. (1990). Uplift history of South Westland using the fission-track dating technique. New Zealand Journal of Geology and Geophysics, 33(2), 201–204. https://doi.org/10.1080/00288306.1990.10425678
- Shuck, B., Van Avendonk, H., Gulick, S. P., Gurnis, M., Sutherland, R., Stock, J., et al. (2021). Strike-slip enables subduction initiation beneath a failed rift: New seismic constraints from Puysegur Margin, New Zealand. *Tectonics*, 40(5), e2020TC006436. https://doi.org/10.1029/
- Sieh, K., Jones, L., Hauksson, E., Hudnut, K., Eberhart-Phillips, D., Heaton, T., et al. (1993). Near-field investigations of the Landers earthquake sequence, April to July 1992. Science, 260(5105), 171–176. https://doi.org/10.1126/science.260.5105.171
- Sláma, J., Košler, J., Condon, D. J., Crowley, J. L., Gerdes, A., Hanchar, J. M., et al. (2008). Plešovice zircon—A new natural reference material for U–Pb and Hf isotopic microanalysis. *Chemical Geology*, 249(1–2), 1–35. https://doi.org/10.1016/j.chemgeo.2007.11.005
- Smith, M., Chantraprasert, S., Morley, C. K., & Cartwright, I. (2007). Structural geometry and timing of deformation in the Chainat duplex, Thailand. *Geological Society, London, Special Publications*, 290(1), 305–323. https://doi.org/10.1144/sp290.11
- Stacey, J. S., & Kramers, J. D. (1975). Approximation of terrestrial lead isotope evolution by a two-stage model. *Earth and Planetary Science Letters*, 26(2), 207–221. https://doi.org/10.1016/0012-821x(75)90088-6
- Stern, T., Okaya, D., Kleffmann, S., Scherwath, M., Henrys, S., & Davey, F. (2007). Geophysical exploration and dynamics of the Alpine Fault Zone. In D. Okaya, T. Stern, & F. Davey (Eds.), A Continental Plate Bounday: Tectonics at South Island, New Zealand, Geophysical Monograph Series (Vol. 175, pp. 207–233). American Geophysical Union. https://doi.org/10.1029/175gm11
- Stirling, M., McVerry, G., Gerstenberger, M., Litchfield, N., Van Dissen, R., Berryman, K., et al. (2012). National seismic hazard model for New Zealand: 2010 update. Bulletin of the Seismological Society of America, 102(4), 1514–1542. https://doi.org/10.1785/0120110170
- Stirling, M. W., Litchfield, N. J., Villamor, P., Van Dissen, R. J., Nicol, A., Pettinga, J., et al. (2017). The M<sub>w</sub> 7.8 2016 Kaikōura earthquake: Surface rupture and seismic hazard context. *Bulletin of the New Zealand Society for Earthquake Engineering*, 50(20), 73–84.
- Stirling, M. W., Wesnousky, S. G., & Shimazaki, K. (1996). Fault trace complexity, cumulative slip, and the shape of the magnitude-frequency distribution for strike-slip faults: A global survey. Geophysical Journal International, 124(3), 833–868. https://doi.org/10.1111/j.1365-246x. 1996.tb05641.x
- Stock, J., & Molnar, P. (1982). Uncertainties in the relative positions of the Australia, Antarctica, Lord Howe, and Pacific plates since the Late Cretaceous. *Journal of Geophysical Research*, 87(B6), 4697–4714. https://doi.org/10.1029/jb087jb06p04697
- Sutherland, R. (1994). Displacement since the Pliocene along the southern section of the Alpine Fault, New Zealand. *Geology*, 22(4), 327–330. https://doi.org/10.1130/0091-7613(1994)022<0327:dstpat>2.3.co;2
- Sutherland, R., Berryman, K., & Norris, R. (2006). Quaternary slip rate and geomorphology of the Alpine fault: Implications for kinematics and seismic hazard in southwest New Zealand. *Geological Society of America Bulletin*, 118(3–4), 464–474. https://doi.org/10.1130/b25627.1
- Sutherland, R., Davey, F., & Beavan, J. (2000). Plate boundary deformation in South Island, New Zealand, is related to inherited lithospheric structure. Earth and Planetary Science Letters, 177(3–4), 141–151. https://doi.org/10.1016/s0012-821x(00)00043-1
- Sutherland, R., Eberhart-Phillips, D., Harris, R. A., Stern, T., Beavan, J., Ellis, S., et al. (2007). Do great earthquakes occur on the Alpine fault in central South Island, New Zealand? In D. Okaya, T. Stern, & F. Davey (Eds.), A Continental Plate Bounday: Tectonics at South Island, New Zealand, Geophysical Monograph Series (Vol. 175, pp. 175–273). American Geophysical Union. https://doi.org/10.1029/175gm12
- Sutherland, R., Gurnis, M., Kamp, P. J., & House, M. A. (2009). Regional exhumation history of brittle crust during subduction initiation, Fiordland, southwest New Zealand, and implications for thermochronologic sampling and analysis strategies. *Geosphere*, 5(5), 409–425. https://doi.org/10.1130/ges00225.sa1
- Sutherland, R., Hollis, C. J., Nathan, S., Strong, C. P., & Wilson, G. J. (1996). Age of Jackson Formation proves late Cenozoic allochthony in South Westland, New Zealand. New Zealand Journal of Geology and Geophysics, 39(4), 559–563. https://doi.org/10.1080/00288306.1996. 9514733
- Sutherland, R., & Melhuish, A. (2000). Formation and evolution of the Solander Basin, southwestern South Island, New Zealand, controlled by a major fault in continental crust and upper mantle. *Tectonics*, 19(1), 44–61. https://doi.org/10.1029/1999tc900048

MERE ET AL. 32 of 34



# Geochemistry, Geophysics, Geosystems

- 10.1029/2024GC011839
- Sutherland, R., & Norris, R. J. (1995). Late Quaternary displacement rate, paleoseismicity, and geomorphic evolution of the Alpine Fault: Evidence from Hokuri Creek, South Westland, New Zealand. New Zealand Journal of Geology and Geophysics, 38(4), 419–430. https://doi.org/10.1080/00288306.1995.9514669
- Swanson, M. T. (1989). Sidewall ripouts in strike-slip faults. Journal of Structural Geology, 11(8), 933–948. https://doi.org/10.1016/0191-8141 (89)90045-x
- Swanson, M. T. (2005). Geometry and kinematics of adhesive wear in brittle strike-slip fault zones. *Journal of Structural Geology*, 27(5), 871–887. https://doi.org/10.1016/j.jsg.2004.11.009
- Tchalenko, J. S. (1970). Similarities between shear zones of different magnitudes. Geological Society of America Bulletin, 81(6), 1625–1640. https://doi.org/10.1130/0016-7606(1970)81[1625:sbszod]2.0.co;2
- Tchalenko, J. S., & Ambraseys, N. N. (1970). Structural analysis of the Dasht-e Bayaz (Iran) earthquake fractures. Geological Society of America Bulletin, 81(1), 41–60. https://doi.org/10.1130/0016-7606(1970)81[41:saotdb]2.0.co;2
- Tchalenko, J. S., & Berberian, M. (1975). Dasht-e Bayaz fault, Iran: Earthquake and earlier related structures in bed rock. Geological Society of America Bulletin, 86(5), 703–709.
- Tera, F., & Wasserburg, G. J. (1972). U-Th-Pb systematics in three Apollo 14 basalts and the problem of initial Pb in lunar rocks. Earth and Planetary Science Letters, 14(3), 281–304. https://doi.org/10.1016/0012-821x(72)90128-8
- Thiele, S. T., Grose, L., Samsu, A., Micklethwaite, S., Vollgger, S. A., & Cruden, A. R. (2017). Rapid, semi-automatic fracture and contact mapping for point clouds, images and geophysical data. Solid Earth, 8(6), 1241–1253. https://doi.org/10.5194/se-8-1241-2017
- Tippett, J. M., & Kamp, P. J. (1993). Fission track analysis of the late Cenozoic vertical kinematics of continental Pacific crust, South Island, New Zealand, Journal of Geophysical Research, 98(B9), 16119–16148, https://doi.org/10.1029/92jb02115
- Toy, V. G., Ritchie, S., & Sibson, R. H. (2011). Diverse habitats of pseudotachylytes in the Alpine Fault Zone and relationships to current seismicity. *Geological Society, London, Special Publications*, 359(1), 115–133. https://doi.org/10.1144/sp359.7
- Toy, V. G., Sutherland, R., Townend, J., Allen, M. J., Becroft, L., Boles, A., et al. (2017). Bedrock geology of DFDP-2B, central Alpine Fault, New Zealand. New Zealand Journal of Geology and Geophysics, 60(4), 497–518. https://doi.org/10.1080/00288306.2017.1375533
- Tulloch, A. J., & Challis, G. A. (2000). Emplacement depths of Paleozoic-Mesozoic plutons from western New Zealand estimated by hornblende-AI geobarometry. New Zealand Journal of Geology and Geophysics, 43(4), 555–567. https://doi.org/10.1080/00288306.2000.9514908
- Tulloch, A. J., Ireland, T. R., Kimbrough, D. L., Griffin, W. L., & Ramezani, J. (2011). Autochthonous inheritance of zircon through Cretaceous partial melting of Carboniferous plutons: The Arthur River Complex, Fiordland, New Zealand. Contributions to Mineralogy and Petrology, 161(3), 401–421. https://doi.org/10.1007/s00410-010-0539-6
- Tulloch, A. J., & Kimbrough, D. L. (1989). The Paparoa metamorphic core complex, New Zealand: Cretaceous extension associated with fragmeotation of the Pacific margin of Gondwana. *Tectonics*, 8(6), 1217–1234. https://doi.org/10.1029/tc008i006p01217
- Tulloch, A. J., & Kimbrough, D. L. (2003). Paired plutonic belts in convergent margins and the development of high Sr/Y magmatism: Peninsular Ranges Batholith of Baja California and Median Batholith of New Zealand. In S. E. Johnson, S. R. Paterson, J. M. Fletcher, G. H. Girty, D. L. Kimbrough, & A. Martin-Barajas (Eds.), Tectonic evolution of northwestern Mexico and the southwestern USA, Geological Society of America Special Paper (Vol. 374, pp. 275–295).
- Tulloch, A. J., Ramezani, J., Kimbrough, D. L., Faure, K., & Allibone, A. H. (2009). U-Pb geochronology of mid-Paleozoic plutonism in western New Zealand: Implications for S-type granite generation and growth of the east Gondwana margin. *Geological Society of America Bulletin*, 121(9–10), 1236–1261. https://doi.org/10.1130/b26272.1
- Turnbull, I. M. (2000). Geology of the Wakatipu area, Geological Map 20. scale 1:250,000 (p. 74). New Zealand Institute of Geological and Nuclear Sciences.
- Turnbull, I. M., & Allibone, A. H., & (compilers). (2003). Geology of the Murihiku area (external link). 1:250 000 geological map 20 (p. 74). Institute of Geological & Nuclear Sciences Limited. + 1 sheet.
- Turnbull, I. M., Allibone, A. H., & Jongens, R. (2010). Geology of the Fiordland area, Geological Map 17. scale 1:250,000 (p. 97). New Zealand Institute of Geological and Nuclear Sciences.
- Turnbull, I. M., Barry, J. M., Carter, R. M., & Norris, R. J. (1975). The Bobs Cove beds and their relationship to the Moonlight Fault Zone. *Journal of the Royal Society of New Zealand*, 5(4), 355–394. https://doi.org/10.1080/03036758.1975.10419360
- Turnbull, I. M., & Uruski, C. I. (1995). Geology of the Monowai Waitutu area, Geological Map 19. scale 1:50,000 (p. 68). New Zealand Institute of Geological and Nuclear Sciences.
- Turnbull, R., Tulloch, A., Ramezani, J., & Jongens, R. (2016). Extension-facilitated pulsed SIA-type "flare-up" magmatism at 370 Ma along the southeast Gondwana margin in New Zealand: Insights from U-Pb geochronology and geochemistry. Bulletin, 128(9–10), 1500–1520. https://doi.org/10.1130/b31426.1
- Turnbull, R. E., Tulloch, A. J., & Ramezani, J. (2013). Zetland Diorite, Karamea Batholith, west Nelson: Field relationships, geochemistry and geochronology demonstrate links to the Carboniferous Tobin Suite. New Zealand Journal of Geology and Geophysics, 56(2), 83–99. https://doi.org/10.1080/00288306.2013.775166
- Upton, P., Song, B. R., & Koons, P. O. (2018). Topographic control on shallow fault structure and strain partitioning near Whataroa, New Zealand demonstrates weak Alpine Fault. New Zealand Journal of Geology and Geophysics, 61(1), 1–8. https://doi.org/10.1080/00288306.2017. 1397706
- Uruski, C. I. (1992). Seismic evidence for dextral wrench faulting on the Moonlight Fault System. New Zealand Geological Survey Record, 44, 69–75.
- Vermeer, J. L., Quigley, M. C., Duffy, B. G., Langridge, R. M., & Pettinga, J. R. (2021). Structure and kinematics of active faulting in the Hope-Kelly and Alpine Fault intersection zone, South Island, New Zealand. *Tectonophysics*, 813, 228928. https://doi.org/10.1016/j.tecto.2021.
- Waight, T. E., Weaver, S. D., Ireland, T. R., Maas, R., Muir, R. J., & Shelley, D. (1997). Field characteristics, petrography, and geochronology of the Hohonu Batholith and the adjacent Granite Hill complex, North Westland, New Zealand. New Zealand Journal of Geology and Geophysics, 40(1), 1–17. https://doi.org/10.1080/00288306.1997.9514736
- Walcott, R. I. (1989). The Paleogene plate boundary through New Zealand (Vol. 43, p. 99). Geological Society of New Zealand miscellaneous publication.
- Wan, Y., Shen, Z. K., Bürgmann, R., Sun, J., & Wang, M. (2016). Fault geometry and slip distribution of the 2008 Mw 7.9 Wenchuan, China earthquake, inferred from GPS and InSAR measurements. *Geophysical Journal International*, ggw421.
- Ward, C. M. (1984). Geology of the Dusky Sound area, Fiordland, with emphasis on the structural-metamorphic development of some porphyroblastic staurolite pelites (Unpublished PhD thesis). University of Otago.

MERE ET AL. 33 of 34



# Geochemistry, Geophysics, Geosystems

- 10.1029/2024GC011839
- Warren-Smith, E., Lamb, S., Seward, D., Smith, E., Herman, F., & Stern, T. (2016). Thermochronological evidence of a low-angle, mid-crustal detachment plane beneath the central S outh I sland, N ew Z ealand. *Geochemistry, Geophysics, Geosystems*, 17(10), 4212–4235. https://doi.org/10.1002/2016gc006402
- Warren-Smith, E., Townend, J., Chamberlain, C. J., Boulton, C., & Michailos, K. (2022). Heterogeneity in microseismicity and stress near rupture-limiting section boundaries along the late-interseismic alpine fault. *Journal of Geophysical Research: Solid Earth*, 127(10), e2022JB025219. https://doi.org/10.1029/2022jb025219
- Watson, E. B. (1979). Zircon saturation in felsic liquids: Experimental results and applications to trace element geochemistry. *Contributions to Mineralogy and Petrology*, 70(4), 407–419. https://doi.org/10.1007/bf00371047
- Watson, E. B., & Harrison, T. M. (1983). Zircon saturation revisited: Temperature and composition effects in a variety of crustal magma types. Earth and Planetary Science Letters, 64(2), 295–304. https://doi.org/10.1016/0012-821x(83)90211-x
- Wellman, H. W. (1956). Structural Outline of New Zealand. In Bulletin (Vol. 121, p. 36). Department of Scientific and Industrial Research.
- Wellman, H. W., & Wilson, A. T. (1964). Notes on the geology and archaeology of the Martins Bay district. New Zealand Journal of Geology and Geophysics, 7(4), 702–721. https://doi.org/10.1080/00288306.1964.10428126
- Wells, A., Yetton, M. D., Duncan, R. P., & Stewart, G. H. (1999). Prehistoric dates of the most recent Alpine fault earthquakes, New Zealand. Geology, 27(11), 995–998. https://doi.org/10.1130/0091-7613(1999)027<0995;pdotmr>2.3.co;2
- Wesnousky, S. G. (1988). Seismological and structural evolution of strike-slip faults. *Nature*, 335(6188), 340–343. https://doi.org/10.1038/
- Wesnousky, S. G. (2006). Predicting the endpoints of earthquake ruptures. Nature, 444(7117), 358-360. https://doi.org/10.1038/nature05275
- Whalen, J. B., Currie, K. L., & Chappell, B. W. (1987). A-type granites: Geochemical characteristics, discrimination and petrogenesis. Contributions to Mineralogy and Petrology, 95(4), 407–419. https://doi.org/10.1007/bf00402202
- Whitney, D. L., & Evans, B. W. (2010). Abbreviations for names of rock-forming minerals. American Mineralogist, 95(1), 185–187. https://doi.org/10.2138/am.2010.3371
- Wiedenbeck, M. A. P. C., Alle, P., Corfu, F. Y., Griffin, W. L., Meier, M., Oberli, F., et al. (1995). Three natural zircon standards for U-Th-Pb, Lu-Hf, trace element and REE analyses. *Geostandards Newsletter*, 19(1), 1–23. https://doi.org/10.1111/j.1751-908x.1995.tb00147.x
- Williams, P. W., McGlone, M., Neil, H., & Zhao, J. X. (2015). A review of New Zealand palaeoclimate from the Last Interglacial to the global Last Glacial Maximum. *Quaternary Science Reviews*, 110, 92–106. https://doi.org/10.1016/j.quascirev.2014.12.017
- Wood, B. L. (1972). Metamorphosed ultramafites and associated formations near Milford Sound, New Zealand. New Zealand Journal of Geology and Geophysics, 15(1), 88–128. https://doi.org/10.1080/00288306.1972.10423948
- Yakymchuk, C., Kirkland, C. L., & Clark, C. (2018). Th/U ratios in metamorphic zircon. *Journal of Metamorphic Geology*, 36(6), 715–737. https://doi.org/10.1111/jmg.12307

MERE ET AL. 34 of 34